

Investigation and sensitivity analysis of a mechanistic phytoplankton model implemented in a new modular numerical tool (Eco3M) dedicated to biogeochemical modelling

Melika Baklouti ^{a,b,*}, Vincent Faure ^{b,c}, Lionel Pawlowski ^d, Antoine Sciandra ^e

^a Institut de Recherche pour le Développement, UR CYROCO, Campus de Luminy, case 901, F-13288 Marseille, France

^b Laboratoire d'Océanographie et de Biogéochimie, UMR 6535, Campus de Luminy, case 901, F-13288 Marseille, France

^c Institut de Recherche pour le Développement, UR CAMELIA SME, rue de la Batterie des Lions, F-13007 Marseille, France

^d Monterey Bay Aquarium Research Institute, 7700 Sandholt Road, Moss Landing, CA 95039-9644, USA

^e LOV, UMR 7093, Station Zoologique, B.P. 28, 06234 Villefranche-sur-mer, France

Received 11 October 2005; received in revised form 19 May 2006; accepted 29 May 2006

Available online 24 August 2006

Abstract

A new class of phytoplankton models with a mechanistic basis has been presented in a companion paper (Baklouti, M., Diaz, F., Pinazo, C., Faure, V., Queguiner, B., 2006. Investigation of mechanistic formulations depicting phytoplankton dynamics for models of marine pelagic ecosystems. *Progress in Oceanography*). It is the default class of models implemented in our new numerical tool *Eco3M*, which is dedicated to *Ecological, Mechanistic and Modular Modelling*. A brief overview of its main features is given in Section 2 of the present paper. In the next sections, a particular phytoplankton model among the aforementioned class has been tested with special emphasis on the mechanistic photosynthesis component relating the photosynthetic rate to the proportion of open photosystems II. The present study encompasses several essential steps that are inherent to any modelling, including model reduction, model sensitivity analysis and comparison of model outputs with experiments. The global sensitivity analysis of the plankton model for one-at-a-time parameter perturbations revealed a restricted set of parameters having major influence on the model outputs. Sensitivity tests involving simultaneous parameter perturbations within the range actually encountered in the literature provided a confidence interval for the outputs. Chemostat experiments performed on nitrate-limited diatoms grown under low (LL) and high-light (HL) conditions have been used for comparison with model outputs. The good fit between measured data and model outputs using the same parameter values in both the LL and HL cases demonstrates the ability of our model to represent the main features of phytoplankton dynamics including photoacclimation. Finally, *Eco3M* is ultimately intended to include explicit bacterial and zooplankton compartments, as well as to be coupled with ocean circulation models, but the intrinsic behavior of the phytoplankton model has been investigated first, independently of physical forcing.

© 2006 Elsevier Ltd. All rights reserved.

Keywords: Ecological modelling; Phytoplankton; Mechanistic formulations; Sensitivity analysis

* Corresponding author. Tel.: +33 491829374.

E-mail address: baklouti@com.univ-mrs.fr (M. Baklouti).

1. Introduction

A new class of multi-element and multi-species phytoplankton models has been elaborated and presented in a companion paper (Baklouti et al., 2006). It is the result of an extensive investigation of literature in order to assess the state-of-the-art in biogeochemical modelling for some of the main processes driving phytoplankton dynamics. Particular attention was paid to mechanistic formulations when they were available, since (i) they represent biogeochemical processes in terms of underlying mechanisms, (ii) they involve, at least partially, physiological parameters that have a restricted range of values (Baird et al., 2004) and (iii) they reduce the need for extrapolation of model parameters in data-poor regions (Baird et al., 2003).

The present class of model is ultimately to be coupled with ocean circulation models to quantify biomass and nutrient variability induced at regional and/or basin scales by seasonal or global changes and by human activities. For this purpose, a new numerical tool for *Ecological, Mechanistic and Modular Modelling (Eco3M)* has been conceived and the present paper gives a brief overview of its fundamental principles. This new numerical tool has been devised to handle multi-element and multi-species biogeochemical models with the main objective that it be wholly modular in regard to the state variables and the associated models for biogeochemical processes. Variables or processes can therefore be added or subtracted with great simplicity. *Eco3M* is also deliberately free from any physical model, but can be coupled to any of them provided a specific interface is created.

Although many biogeochemical models are being widely used in combination with general circulation models, relatively little work has been done toward understanding their intrinsic dynamics Lima et al., 2002 or their sensitivity in respect to parameter perturbations, independent of physical forcing. Due to the wide ranges of most of the parameters involved, biogeochemical models can display significant differences in their outputs according to the values selected. In addition, several expressions are available in the literature to describe a single biogeochemical process and a wide range of dynamic behaviors arise from the use of one or another of these formulations.

In this context, we provide a worked example of model testing encompassing several essential steps. The first is model reduction with dedicated techniques. Beyond simplification, these methods are intended to build models with an efficient structure devoid of redundancy and, therefore, more comprehensible regarding the important relationships within the whole system. Among them, the perturbation methods focus on models that display multiple time-scale behavior in order to separate distinct types of response (Robertson and Cameron, 1997). The reduced model can, therefore, be fully adapted in order to represent the phenomena occurring at the time-scale of interest. Similarly, model reduction can be achieved through the variable aggregation method. That consists in defining a reduced number of global variables, which are functions of the state variables of the original model, to provide a simplified system of equations (Auger and Lett, 2003). Again, the underlying idea is to take advantage of the different time scales that are involved in the model. Sensitivity analysis (SA) is also an important step in model testing, with the aims of prioritizing data acquisition and improving the structure and parameterization of the model where necessary.

In practice, SA allows estimation of the change in the model solution given an estimated error in the model parameters. Considering that a very sensitive solution, where large changes in the solution result from small changes in the parameter estimates, is not desirable (Seferlis and Hrymak, 1996), the identification of the most influential parameter(s) is very useful. This can help in refining some experimental techniques dedicated to the determination of such parameters or suggest model changes to make it more robust. In practice, sensitivity analysis can be divided in two main categories (i) local sensitivity methods that calculate the local gradients of the solution with respect to infinitesimal parameter variations and (ii) global sensitivity methods that determine the behavior of the solution under parameter perturbations of arbitrary magnitude. In addition to one-at-a-time parameter perturbations, SA can be widened to include simultaneous parameter perturbations. As a matter of fact, even when the sensitivity of an output to every individual parameter is investigated, potentially important effects of interactions between parameters are not revealed. In other words, the joint effect produced by several parameters may be greater than the sum of their individual effects. Furthermore, significant interactions may arise among what were not otherwise considered highly sensitive parameters. These limitations of one-at-a-time perturbation analysis, particularly for large complex models, point the need for alternative methods in which the parameters vary all together Newham et al., 2003. Finally, the comparison with

laboratory and/or field experiments is obviously the best way to assess model ability to represent modeled phenomena. Unfortunately, this is often difficult to achieve due to the lack of data (especially dynamic data) or to data inappropriate for the model under investigation.

The present paper focuses on a particular phytoplankton model among the class of biogeochemical models presented in Baklouti et al. (2006). In accordance with the aforementioned steps of model testing, this study aims at analysis of its intrinsic dynamics for structural insight and possible model reduction, as well as at identifying the most sensitive parameters through a global sensitivity analysis. This paper is organized as follows: First, the dynamic Han (2002) photosynthesis model has been reduced by variable aggregation, accounting for the large differences in the time-scales involved. Second, as several formulations for quota models are available in the literature, some of them have been compared. Afterwards, the sensitivity of the phytoplankton model has been tested through one-at-a-time parameter perturbations to identify the parameters mainly sensitive in regard to model output. We have also considered the case where all parameters vary simultaneously within the ranges actually encountered in the literature, in order to obtain realistic confidence intervals for our model outputs. Finally, model outputs have been compared with continuous chemostat experiments on light-and nitrate-limited *Thalassiosira weissflogii*.

2. Presentation of the new numerical tool *Eco3M*

It is likely that the first version of a new model will be submitted to many changes in the future, not only to improve the existing version, but to enlarge the field of possible applications by adding new variables or new biogeochemical processes. This necessary evolution led us to give particular attention to the modularity of our numerical code, thereby anticipating future improvements. In order to reach this objective, *Eco3M* has been developed in *fortran 90-95*, and we have used some powerful characteristics of this language such as derived types, modules and dynamic memory through pointers. Besides, the numerical code is written with matrices and vectors of un-fixed size that allow as many state variables as desired.

Each state variable in *Eco3M* is identified by three components: (i) the group it belongs to (among phytoplankton, dissolved inorganic matter, detrital matter, . . .), (ii) its sub-group (i.e. the functional group or the species), and (iii) the element it is expressed in (among N, P, Si, Fe, . . .). Thus, the producers, consumers and mineralisers have dynamically varying C:N:P:Si:(. . .) ratios. The nature and the number (n_v) of state of variables are defined by the modeller and are regrouped in vector $\mathbf{x} : \mathbf{x} = (x_i)_{1 \leq i \leq n_v}$. Moreover, though in the present study state variables are independent from spatial coordinates, three dimensional variables can be used as well.

One of the more concise methods for defining material fluxes between state variables in a complex model is to build a matrix of biogeochemical fluxes, here denoted MF. The elements of the square matrix MF of size (n_v, n_v) contain the values of the material fluxes between state variables when this is pertinent and zero otherwise. A specific detail is that MF(i, j) corresponds to the algebraic material flux from $x(i)$ to $x(j)$, which is either positive or negative and necessarily opposite to the flux from $x(j)$ to $x(i)$. Hence, in order to avoid superfluous storage and calculus in the numerical code, MF is restricted to a triangular superior matrix (with nil terms on the diagonal). Moreover, in order to take into account the closure terms inherent to any model, a flux vector VF contains the material fluxes involving a single state-variable (the origin or the destination of this flux being a variable which is not explicitly represented in the model). Hence, VF has dimension n_v .

Each element of matrix MF is subdivided into two components: (i) the nature of the flux represented through the name of the analytical function associated to the biogeochemical process between both state variables and (ii) the amount of this flux. We have also considered the case where the material flux between two state variables is the result of several simultaneous biogeochemical processes. Finally, from MF and VF, the algebraic sum of gains and losses (TF) for each variable i can be calculated at each time step as follows:

$$\text{TF}(i) = \text{VF}(i) + \sum_{k=1}^{i-1} \text{MF}(k, i) - \sum_{j=i+1}^{n_v} \text{MF}(i, j). \quad (1)$$

A default model is implemented in *Eco3M*, but a different model can easily be introduced through a text file without modifying program sources. In addition, *Eco3M* contains a default library of functions for many biogeochemical processes, but new functions can also be added easily.

3. The photosynthesis model

3.1. The dynamic model

Han's (2002) mechanistic formulation is used to model photosynthesis. It includes algal photoinhibition induced by photodamage to photosystems II (PSIIs). In this model, each PSII is assumed to be in one of three possible states, namely open (i.e. reactive), closed (i.e. already activated), or photoinhibited. The respective proportions n_o , n_c and n_{in} of PSIIs in each state vary with time according to irradiance, E , fluctuations, while the sum ($n_o + n_c + n_{in}$) remains equal to 1. A schematic presentation of the transitions between the three states is presented as Eq. (2). It involves k_d ($= k_d^H \cdot \sigma \cdot E$) and k_r , the rate constants (in s^{-1}) relative to PSII damage and repair, respectively. Parameter σ stands for the absorption cross-section of PSII, k_d^H for a dimensionless damage rate constant and τ for the turnover time of the electron transport chain. More details of the physiology underlying the assumptions made in this model can be found in Han (2002)



The dynamic evolution of (n_o, n_{in}) is derived from the assumption of first order kinetics and from the application of the mass action law. This leads to the following differential equations for (n_o, n_{in}) :

$$\frac{dn_o}{dt} = -\sigma E n_o + \frac{(1 - n_o - n_{in})}{\tau}, \quad (3a)$$

$$\frac{dn_{in}}{dt} = -k_r n_{in} + k_d^H \sigma E (1 - n_o - n_{in}). \quad (3b)$$

The proportion n_c of closed PSII is therefore easily deduced from:

$$n_c = 1 - n_o - n_{in}. \quad (4)$$

The numerical integration of system (3) provides the time variations of the probability of PSII being open (n_o), which allows calculation of the Chl a-specific primary production rate P^* through Eq. (5). This equation conveys the fact that the quantum yield of carbon fixation is proportional to the PSII probability of being open, i.e. that $\phi^C = n_o \cdot \phi_m^C$ where ϕ_m^C is the maximum quantum yield. In Eq. (5), \bar{a}^* stands for the spectrally-integrated Chl a-specific absorption coefficient over the [400–700] nm range.

$$P^* = \phi \cdot \bar{a}^* \cdot E = n_o \phi_m^C \cdot \bar{a}^* \cdot E. \quad (5)$$

Han's (2002) model involves six parameters, namely σ , τ , ϕ_m^C , \bar{a}^* , k_d^H , k_r , that are not only physiologically meaningful, but are all measurable. Literature was evaluated to provide a range of likely values (see Section 3.2) as well as nominal values for each of them. The latter are given in Table 2 and will be used for each simulation unless noted otherwise. Light/dark circadian cycles are simulated through a time-dependent incident irradiance of period T_p given by Eq. (6). Variable E_m is the irradiance amplitude and β was set to 3.7 for the whole set of simulations presented in this paper with the exception of the chemostat simulations in Section 4.4

$$E = E_m \cdot \exp \left(\beta \cdot \left(\cos \left(\frac{2\pi t}{T_p} \right) - 1 \right) \right). \quad (6)$$

The stiffness of the ODE system (3) is manifest from the presence of time constants that vary over several orders of magnitude. As a consequence, the Jacobian matrix is ill-conditioned, and its condition number increases with irradiance, always being higher than 10^6 over the whole range of depicted irradiances. Since stiff dynamical systems are exceedingly difficult to integrate using standard methods, system (3) has been numerically integrated using a backward differentiation formula (BDF) that is suitable for the numerical integration of such problems (Petzold, 1983). Fig. 1 reports simulated variations of the proportion of open photosystems and of the photosynthesis rate with time for high-light (HL; $E_m = 1000 \mu\text{mol quanta m}^{-2} \text{s}^{-1}$) and low-light (LL; $E_m = 230 \mu\text{mol quanta m}^{-2} \text{s}^{-1}$) cycles. As expected, the proportion of open PSII decreases when light increases and conversely. For the HL simulation, n_o vanishes when the irradiance is near its

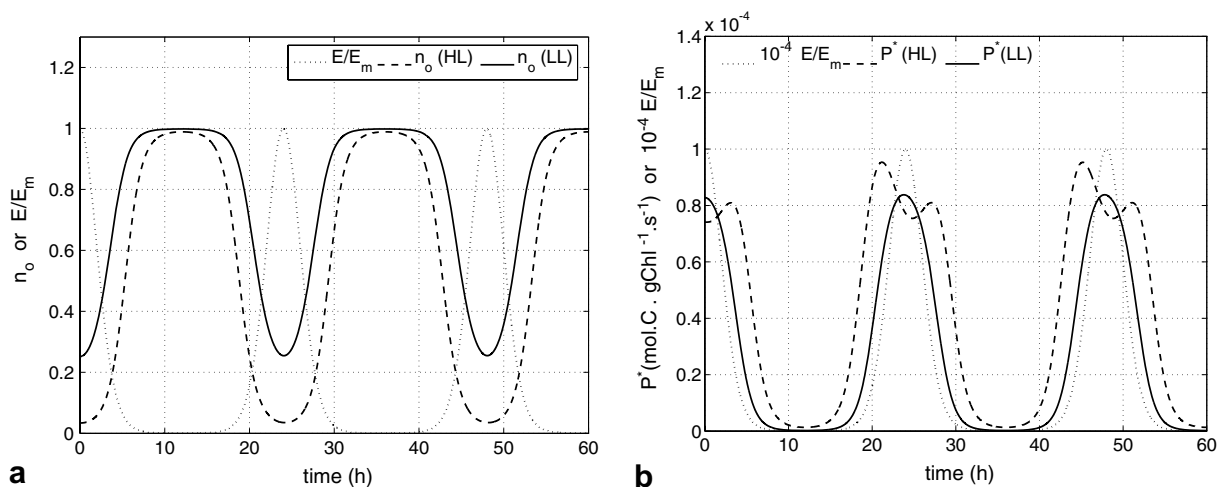


Fig. 1. Dynamic evolution of (a) the proportion n_o of open PSII (b) the photosynthetic rate obtained with two maximum irradiances: $E_m = 230$ (LL) and $E_m = 1000 \mu\text{mol quanta m}^{-2} \text{s}^{-1}$ (HL).

maximum, while the light harvesting complex never saturates in the LL case. The appearance of the photosynthetic rate over light/dark cycles varies greatly depending on E_m . Indeed, for the HL case, photoinhibition is clearly occurring through the local minimum in P^* as E tends toward E_m , while for the LL case, P^* reaches its maximum value near $E = E_m$. Fig. 1b suggests additional comments: First, the shape of the primary production rate over a light/dark cycle is not symmetric because the maximum in irradiance does not coincide with the minimum proportion of open PSII. The lag between them arises from the delay between the increase of irradiance and the reduction of n_o . Second, P^* is not null during the dark period. This artefact is due to the irradiance model (Eq. (6)) in which the minimum value over a cycle is not zero but equal to $E_m \cdot \exp(-2\beta)$.

Considering that the photosynthesis model is intended to be used in a large ecological model and that, in addition, the stiff ordinary differential equation (ODE) system (3) can present problems in getting the solution to converge, a convenient alternative would consist in using the stationary solution of the latter system. Computational costs could therefore be highly reduced. The validity of this approximation will be debated in Section 3.3 after a discussion on the parametrization of the photosynthesis model.

3.2. Parametrization of the photosynthesis model

Table 1 reports the results of our investigation of the literature to obtain likely values for the photosynthetic parameters for different phytoplankton species and different growth environments (culture as well as in situ data). In Han's (2002) model, the PSII damage rate k_d (in s^{-1}) is proportional to the PSII cross-section σ and to the incident irradiance E through:

$$k_d = k_d^H \sigma E. \quad (7)$$

The values of $k_d^H \sigma$ reported in Table 1 are derived from Eq. (7) using values of k_d provided in Baroli and Melis (1996) and Oliver et al. (2003).

From the data reported in Table 1, nominal values and standard deviations for Han's (2002) model parameters were derived and are reported in Table 2. For each parameter p_i , a mean \bar{p}_i which will stand for the p_i nominal value has been computed. These nominal values are used in our simulations unless noted otherwise. Standard deviations have also been calculated from the available set of data. Accounting for the low number of parameter values, the mean has been approximated by $\bar{p}_i = (\max_i(p_i) + \min_i(p_i))/2$, while the standard deviations have been approximated by $(\max_i(p_i) - \min_i(p_i))/4$.

Table 1
Values for the Han (2002) model parameters taken from the literature

Parameter	Details	Value	Reference
\bar{a}^* (m ² (g Chl) ⁻¹)	Natural populations	32	Johnson et al. (2002)
	Oligotrophic	20–40	Babin et al. (1996)
	Natural populations	54–64	Suggett et al. (2001)
$k_d^H \sigma$ (Å ² quanta ⁻¹)	Culture (<i>Dunaliella salina</i>)	2.1×10^{-5}	Baroli and Melis (1996)
	<i>Botryococcus</i>	5.3×10^{-6} – 2.7×10^{-5}	Oliver et al. (2003)
k_r (s ⁻¹)	Higher plants	1.9×10^{-4}	Tyystjarvi and Aro (1996)
	Culture (dark-adapted <i>Dunaliella tertiolecta</i>)	0.7×10^{-4} – 1.8×10^{-4}	Heraud and Beardall (2000)
	Culture (light-adapted <i>Dunaliella tertiolecta</i>)	0.67×10^{-4} – 1.33×10^{-4}	Heraud and Beardall (2000)
	<i>Botryococcus</i>	0.7×10^{-4} – 4.6×10^{-4}	Oliver et al. (2003)
ϕ_m^C (mol C (mol quanta) ⁻¹)	Field (oligotrophic)	5×10^{-3} – 6.2×10^{-2}	Babin et al. (1996)
	Field (mesotrophic)	2×10^{-2} – 3.4×10^{-2}	Babin et al. (1996)
	Field (eutrophic)	4.6×10^{-2} – 5.8×10^{-2}	Babin et al. (1996)
		2×10^{-2} – 8.1×10^{-2}	Moore et al. (2003)
	Culture	8.3×10^{-2} – 10^{-1a}	Modified from Ley and Mauzerall (1982)
σ (Å ² quanta ⁻¹)	Natural phytoplanktonic populations	401–798	Moore et al. (2005)
	Culture (<i>Chlorella pyrenoidosa</i>)	282–350	Kolber et al. (1998)
	Culture	101–1000	Olson et al. (1996)
	Individual algal cells	300–581	Gorbunov et al. (1999)
τ (ms)	Culture (<i>Thalassiosira weissflogii</i>)	2–8	Behrenfeld et al. (1998)
	Culture (<i>Thalassiosira weissflogii</i>)	1.25–7.8	Laney et al. (2005)
	Culture (<i>Chlorella</i>)	2.3–10	Kaňa et al. (2002)

Parameter definitions are provided in Table 2.

^a Oxygen maximum quantum yields transformed in carbon quantum yields using the value of 1.2 for the photosynthetic quotient.

3.3. Comparison of the dynamic and the stationary models

The steady-state solution (n_o^s, n_c^s, n_m^s) of system (3) can be derived easily. Accounting for Eq. (5), the stationary chlorophyll-specific photosynthesis rate is given by the following equation:

$$P^{*s} = \frac{\phi_m \cdot \bar{a}^* \cdot E}{1 + \sigma \tau E + (k_d^H/k_r)(\sigma E)^2 \tau}. \quad (8)$$

The maximum chlorophyll-specific primary production rate P_m^* and the corresponding irradiance E_{\max} are then given by:

$$P_m^* = \frac{\bar{a}^* \cdot \phi_m^C / \sigma}{2\sqrt{(K\tau)} + \tau}, \quad E_{\max} = \frac{1}{\sigma\sqrt{K\tau}}, \quad (9)$$

where K is the ratio k_d^H/k_r .

We now investigate the differences between the Han's model stationary and dynamic photosynthetic rates by comparing the outputs provided by the dynamic (hereafter D) solution of system (3) to the ones provided by the stationary (hereafter S) solution (Eq. (8)). The time-dependent irradiance is still given by Eq. (6), and two cases have again been considered corresponding to low (LL) and high (HL) irradiance amplitudes: $E_m = 230$ and $1000 \mu\text{mol quanta m}^{-2} \text{s}^{-1}$, respectively. The nominal parameter values given in Table 2 were used, while the initial values of n_o and n_m were provided by the stationary solution.

Time variations of $P^*(S)$ and $P^*(D)$ are plotted in Figs. 2a and b, respectively, for the LL and HL cases. Unlike the stationary solutions, the dynamic solutions in both the HL and LL cases exhibit asymmetric shapes over a light/dark cycle, and in the LL case this can be associated with the afternoon depression in photosynthesis. Moreover, contrary to the HL case, the difference between $P^*(S)$ and $P^*(D)$ in the LL case is weak, indicating that the steady-state is reached quite immediately over most of the light/dark cycle. At this stage,

Table 2
Han's (2002) model nominal parameter values used in simulations

Parameter	Symbol	Nominal value	Standard deviation (SD)	Normalized SD
[400;700 nm] mean Chla-specific absorption coefficient	\bar{a}^*	42	11	26
Dimensionless PSII damage rate	k_d^H	4.5×10^{-8a}	1.8×10^{-8}	40
Repair rate of damaged PSII	k_r	2.6×10^{-4}	9.8×10^{-5}	38
Maximum quantum yield of carbon fixation	ϕ_m^C	5.2×10^{-2}	2.4×10^{-2}	46
Effective cross-section of PSII	σ	550	225	41
Turnover time of electron transfer	τ	5.6×10^{-3}	2.2×10^{-3}	39

^a The nominal value of k_d^H is obtained by dividing the nominal value of $k_d^H \sigma$ by the nominal value of σ . Parameter units are given in Table 1.

the main question to address is whether or not the difference arising from the use of the stationary instead of the dynamic model over large time scales will induce a significant error in the assessment of the primary production per biomass per year for example. To attempt to answer this question, the relative (ε) and integrated relative (ε_i) errors between the dynamic (D) and stationary (S) chlorophyll-specific primary production rates have been calculated as follows:

$$\varepsilon(t) = \frac{P_D^*(t) - P_S^*(t)}{P_D^*(t)}, \quad (10)$$

$$\varepsilon_i = \int_0^T \varepsilon(t) dt. \quad (11)$$

In Fig. 3a, the relative error of the photosynthetic rate $\varepsilon(t)$ as well as the variations of the absolute value of the light derivative with time $|dE/dt|$ has been reported for both the LL and the HL cases. In both cases, the error increases with the light derivative. Similarly, it has also been checked that when the period of the light/dark cycles is increased, which means that light variations with time become slower, the lag between the stationary and the dynamic solutions is reduced for both the HL and LL experiments (results not shown). Fig. 3a also reveals that the error pattern $\varepsilon(t)$ is not symmetric over a light cycle and that its negative and positive contributions do not cancel each other out over a cycle. The latter point is better illustrated in Fig. 3b by the

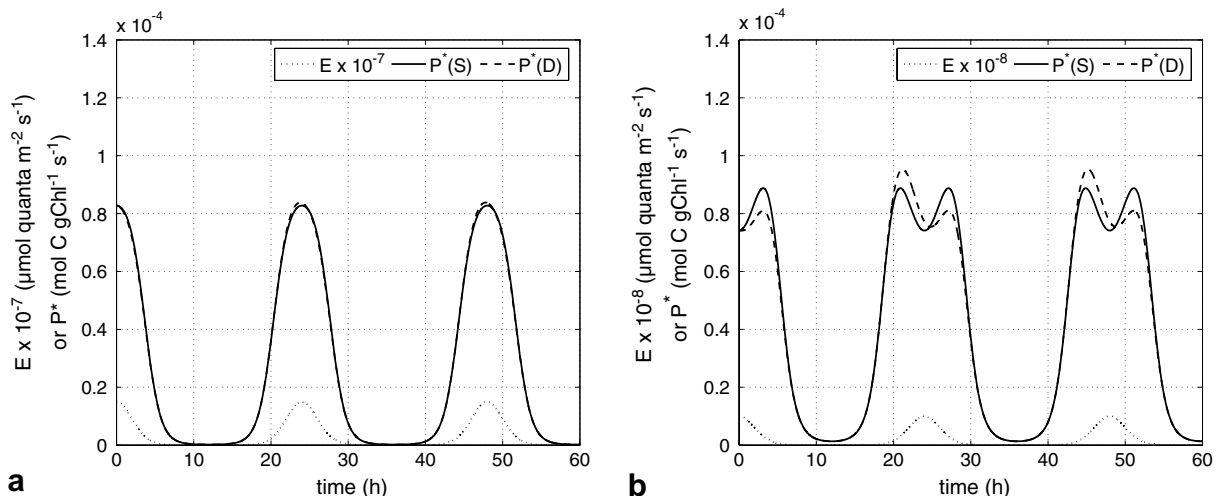


Fig. 2. Comparison of photosynthetic rates derived from stationary and dynamic solutions for two maximum irradiances: (a) $E_m = 230$ and (b) $E_m = 1000 \mu\text{mol quanta m}^{-2} \text{s}^{-1}$.

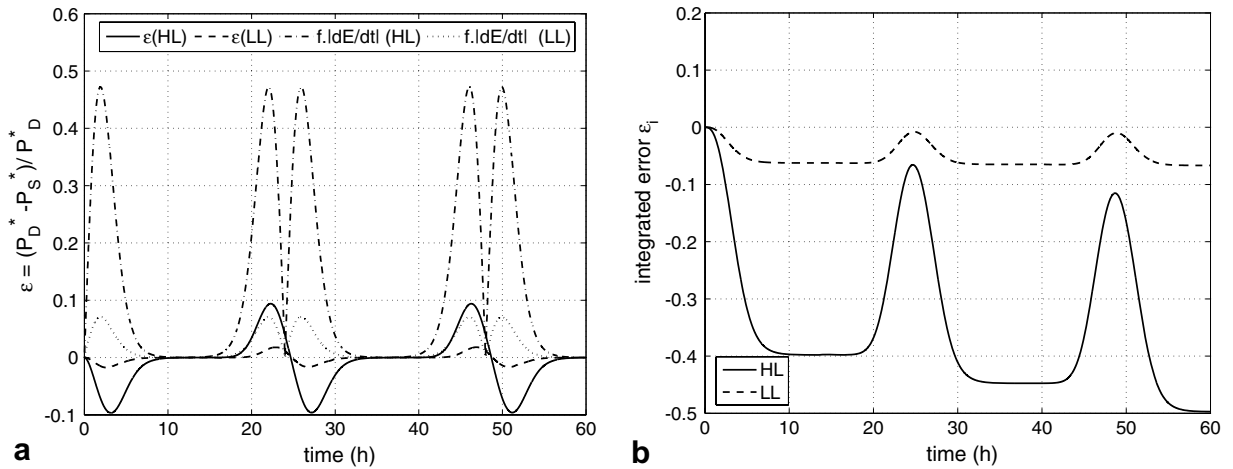


Fig. 3. Dynamic (a) and integrated (b) errors between the stationary and the dynamic solutions for the two maximum irradiances. In figure (a), the absolute value of the light derivative $|dE/dt|$ has been scaled by parameter $f = 1/100$.

unbounded increase of the integrated error ε_i in absolute value. The asymmetry of $\varepsilon(t)$ (Fig. 3a) is due to the fact that the repair (k_r) and damage ($k_d^H \sigma E$) rates are not equal. As a matter of fact, the error which is generated by the delay in reaching the steady-state will depend upon the parameter values, especially on k_r and $k_d^H \sigma E$. The latter two rates indeed control the whole system dynamics, as they are far weaker than the rates of the two other transformations. In other words, the transformation toward the right side (see Eq. (2)) is controlled by the second step (i.e. $n_c \rightarrow n_{in}$) since $\sigma E \gg k_d^H \sigma E$, while the transformation toward the left side is controlled by the $n_{in} \rightarrow n_c$ step since $\frac{1}{\tau} \gg k_r$. Finally, accounting for the negative sign of the integrated error ε_i , Fig. 3b also indicates that the steady-state solution overestimates the primary production rate.

Thus, the use of the stationary model brings simplicity but also generates errors, as might be expected. The extrapolation of the integrated relative error over a month can amount to an overestimate of 10 % in the chlorophyll-specific photosynthesis rate with the stationary model and the highest irradiance ($E_m = 1000 \mu\text{mol quanta m}^{-2} \text{s}^{-1}$). This error is, however, far less significant for the LL simulation, since light variations are slower, making the steady-state practically attainable within a time step.

In conclusion, the error between the steady-state and the dynamic solutions for Han’s (2002) photosynthesis model mostly depends on the rate at which irradiance varies compared to the rates of the photosystem kinetics. In regions where rapid changes in light-intensity occur due to vertical mixing for instance, the use of the dynamic model is highly recommended, while for slow variation of light, the steady-state model is wholly satisfactory. To avoid this choice, an alternative model has been elaborated, combining simplicity and precision. It can be applied in any light conditions. It is presented in the next section.

3.4. A reduced dynamic model for photosynthesis

The transitions involved in photoproduction (i.e. $n_o \rightleftharpoons n_c$) occur within seconds, much faster than those involved in photoinhibition and repair (i.e. $n_c \rightleftharpoons n_{in}$) that typically take a period in the range of an hour (see parameter values in Table 1). This infers:

$$\sigma E \gg k_d^H \sigma E \quad \text{and} \quad \frac{1}{\tau} \gg k_r. \tag{12}$$

It is, therefore, relevant to consider, as do Klepper et al. (1988), that the equilibrium between the open (n_o) and closed (n_c) photosystems is quite immediately reached, while the transitions $n_c \rightleftharpoons n_{in}$ control the kinetics of the whole system. This yields the following equations after some mathematical transformations involving the aggregate variable $n = n_o + n_c$:

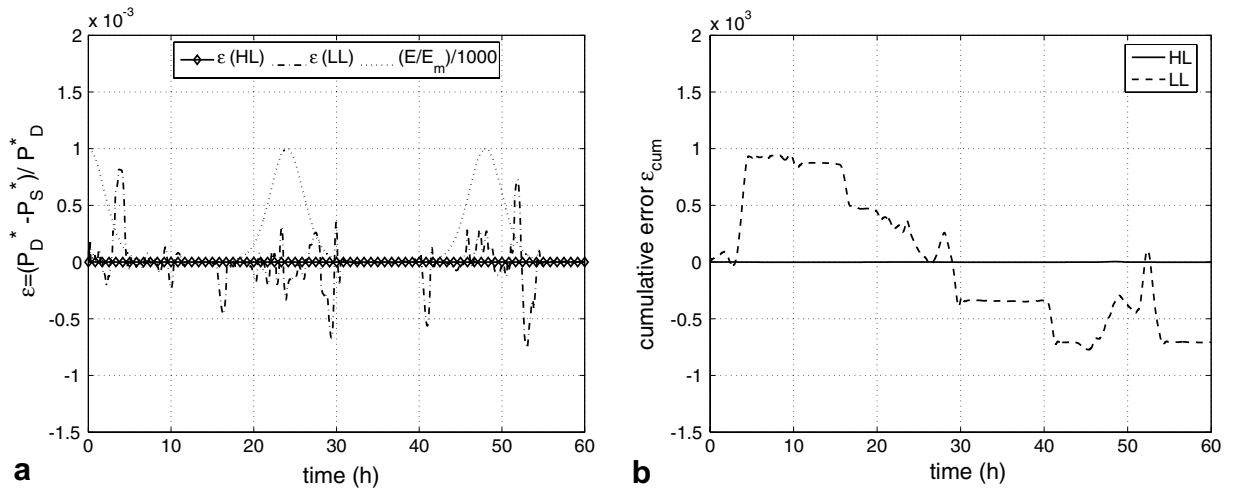


Fig. 4. (a) Dynamic and (b) Integrated errors between the complete and the simplified dynamic solutions for the LL ($E_m = 230 \mu\text{mol quanta m}^{-2} \text{s}^{-1}$) and HL ($E_m = 1000 \mu\text{mol quanta m}^{-2} \text{s}^{-1}$) numerical experiments.

$$n_o = \frac{(1 - n_{in})}{1 + \sigma E \tau}, \quad (13a)$$

$$\frac{dn_{in}}{dt} = \frac{k_d^H (\sigma E)^2 \tau (1 - n_{in})}{1 + \sigma E \tau} - k_r n_{in}. \quad (13b)$$

System (13b) is a reduced version of the complete model given by system (3). Comparison between the complete and the reduced models using the nominal set of parameters given in Table 2 now gives excellent results as shown in Fig. 4 representing the dynamic and integrated, relative photosynthetic rate errors between the two models.

The use of system (13b) instead of (3) offers several advantages in terms of computational costs, as the former contains a single ODE. The numerical integration is also easier because there are no more problems arising from system (3) stiffness. Furthermore, depending on the expression for $E(t)$, an analytic solution of system (13b) can even be calculated.

4. Investigation of a mechanistic phytoplankton model

In the previous sections, the emphasis has been put on one among the key processes driving phytoplankton dynamics, i.e. photosynthesis, and this enabled us to derive a simplified dynamic model for photosynthesis. We will now go further in investigating a complete mechanistic phytoplankton model that is a particular case of the class of biogeochemical models presented in Baklouti et al. (2006).

4.1. The phytoplankton model

The phytoplankton model is depicted in system (14) in which C, Chl and N refer to the phytoplankton internal concentrations in carbon, chlorophyll and nitrogen, respectively. Nitrogen is also considered under four forms, i.e. nitrate (NO_3), ammonium (NH_4), dissolved organic nitrogen (DON) and detrital organic nitrogen (PON). Phytoplankton primary production rate under nutrient-replete conditions (P_{nr}^C) (see Eq. (16)) uses the reduced version of the mechanistic Han (2002) model that has been derived in Section 3.4. The carbon-specific primary production rate P^C is assumed to be a Droop function of the nitrogen-to-carbon ratio (Q) as shown in Eq. (17). The autotrophic respiration formulation (see Eqs. (14b) and (18)) relies on Thornley and Cannell's (2000) model that accounts for the energetic costs r_g , r_{u,NO_3} , $r_{u,\text{N}}$ and $r_{r,\text{N}}$ in terms of carbon associated with the three main activities of phytoplanktonic cells, namely growth, uptake

(of nitrate and other nitrogen sources) and nitrate reduction. It has been hypothesized that the energetic cost of ammonium and DON uptakes are the same, since no data were available for the latter. Phytoplankton mortality is classically represented as a function of the standing phytoplankton biomass through a mortality rate constant m_p . Grazing is not accounted for here, since we aimed at creating a model for investigating the effects of elaborated phytoplankton processes, but it could be implicitly considered through an enhanced mortality term. Nutrient uptake uses the well-known Monod formalism involving the external nutrient concentration and is also controlled by a quota function f_Q^{upt} . The maximum carbon-specific uptake rate V_m is the same for the three nutrients (i.e. NO_3 , NH_4 and DON) and is set proportional to the maximum achievable primary production rate obtained under nutrient replete conditions and to Q_{max} the maximum N:C quota (see Eq. (19)). Moreover, identical affinity constants for ammonium and nitrate can be observed as by Collos et al. (2004). Through Eqs. (20)–(22), uptake is a function of nutrient quota and is, therefore, directly related to the phytoplankton physiological state and indirectly related to irradiance. The model also incorporates that when the maximum internal quota is reached, uptake still proceeds but the excess of nutrient uptake is released in organic form (DON), though nitrite exudation could be included as well. Finally, the inhibition of nitrate uptake by ammonium is also taken into account through the Harrison et al. (1996) formulation (Eq. (20)). The model includes a variable Chl:C ratio using a specific equation devoted to chlorophyll conservation (Eq. (14c)). The latter combines features from models by Geider et al. (1998) and Flynn and Flynn (1998) in order to allow chlorophyll synthesis even when nitrogen net uptake ceases, i.e. when the maximum nitrogen cell quota is reached (see Eqs. (25) and (26)). Finally, the bacterial activity is implicitly considered through a remineralization rate R_{rem} of the dissolved organic compartment, and a detritus breakdown rate of the detrital compartment PON. Further details on these formulations and the underlying mechanisms are provided in the companion paper (Baklouti et al., 2006).

$$\frac{dn_{\text{in}}}{dt} = \frac{k_d^{\text{H}}(\sigma E)^2 \tau (1 - n_{\text{in}})}{1 + \sigma E \tau} - k_r n_{\text{in}}, \quad (14a)$$

$$\frac{dC}{dt} = P_{\text{nr}}^{\text{C}} \cdot f_Q \cdot C - \sum_r R_r - m_p \cdot C, \quad (14b)$$

$$\frac{d\text{Chl}}{dt} = \rho_{\text{Chl}} \cdot V_{\text{chl}} \cdot C - m_p \cdot \text{Chl}, \quad (14c)$$

$$\frac{dN}{dt} = V \cdot f_Q^{\text{upt}} \cdot C - m_p \cdot N, \quad (14d)$$

$$\frac{d\text{NO}_3}{dt} = -V_{\text{NO}_3} \cdot C, \quad (14e)$$

$$\frac{d\text{NH}_4}{dt} = -V_{\text{NH}_4} \cdot C + R_{\text{rem}} \text{DON}, \quad (14f)$$

$$\frac{d\text{DON}}{dt} = (1 - f_Q^{\text{upt}}) \cdot (V_{\text{NO}_3} + V_{\text{NH}_4}) \cdot C - f_Q^{\text{upt}} \cdot V_{\text{DON}} \cdot C - R_{\text{rem}} \text{DON} + R_{\text{bd}} \cdot \text{PON}, \quad (14g)$$

$$\frac{d\text{PON}}{dt} = m_p N - R_{\text{bd}} \cdot \text{PON}. \quad (14h)$$

Growth

$$n_o = \frac{(1 - n_{\text{in}})}{1 + \sigma E \tau}, \quad (15)$$

$$P_{\text{nr}}^{\text{C}} = \bar{a}^* n_o \phi_m^{\text{C}} E \theta, \quad \text{where } \theta = \frac{\text{Chl}}{C}, \quad (16)$$

$$f_Q = 1 - \frac{Q_{\text{min}}}{Q}, \quad \text{where } Q = \frac{N}{C}, \quad (17)$$

$$\sum_r R_r = (r_g \cdot P^{\text{C}} + r_{\text{u,NO}_3} \cdot V_{\text{NO}_3} + r_{\text{u,N}} \cdot (V_{\text{NH}_4} + V_{\text{DON}}) + r_{\text{r,NO}_3} \cdot V_{\text{NO}_3}) \cdot C. \quad (18)$$

Uptake

$$V_m = \bar{a}^* E_k \phi_m^C \theta Q_{\max}, \quad \text{where } E_k = \frac{1}{\sigma \tau}, \quad (19)$$

$$V_{\text{NO}_3} = V_m \cdot \frac{\text{NO}_3}{K_N + \text{NO}_3} \cdot \left(1 - \frac{I_m \cdot \text{NH}_4}{K_I + \text{NH}_4}\right), \quad (20)$$

$$V_{\text{NH}_4} = V_m \cdot \frac{\text{NH}_4}{K_N + \text{NH}_4}, \quad (21)$$

$$V_{\text{DON}} = V_m \cdot \frac{\text{DON}}{K_{\text{DON}} + \text{DON}}, \quad (22)$$

$$V = V_{\text{NO}_3} + V_{\text{NH}_4} + V_{\text{DON}}, \quad (23)$$

$$f_Q^{\text{upt}} = \frac{Q_{\max} - Q}{Q_{\max} - Q_{\min}}. \quad (24)$$

Chlorophyll synthesis

$$\rho_{\text{chl}} = \theta_m^N \frac{P^C}{\bar{a}^* \phi_m^C \theta E} = \theta_m^N n_{\alpha} f_Q, \quad \text{where } P^C = P_{\text{nr}}^C \cdot f_Q, \quad (25)$$

$$V_{\text{chl}} = V \cdot \frac{1 - \theta^N / \theta_m^N}{(1 - \theta^N / \theta_m^N) + 0.05}, \quad \text{where } \theta^N = \frac{\text{Chl}}{\text{N}}. \quad (26)$$

4.2. Preliminary tests

A simulation that will be referred to as the reference simulation in what follows has been conducted using the phytoplankton model described in system (14). Parameter values are taken within realistic ranges that were provided by various literature sources relative to different plankton species and geographical sites (Table 3). For each parameter, mean (nominal value) and standard deviation values have been calculated as in Section 3.2 (see Table 4). Only single values for the autotrophic respiration parameters were found, and arbitrary standard deviations have been associated with them. In this simulation, all the parameters take their nominal values reported in Tables 2 and 4. Arbitrary but realistic initial conditions have been selected that are given in Table 5. Light variations follow Eq. (6) in which the maximum light irradiance E_m has been set to $1150 \mu\text{mol quanta m}^{-2} \text{s}^{-1}$. The reference simulation has been continued until steady-state is reached, approximately 180 days after the beginning of the simulation. The corresponding outputs are presented in Figs. 5a–f. With the nominal set of parameters, phytoplankton carbon (nitrogen) increases during the first 10(6) days and then decreases before stabilization. As intracellular nitrogen concentration decreases prior to carbon concentration, it can be deduced that phytoplankton growth is nutrient-limited rather than light-limited in the present case. After about 45 days, nitrate is exhausted and regeneration becomes the only nitrogen source for phytoplankton. However, the nitrification process has been neglected, which could have been maintained nitrate concentration at low values. Finally, we note that different patterns of biomass and nutrient evolution are observed with other sets of parameters.

4.2.1. Investigating quota functions

We discussed the importance of nutrient quotas to our mechanistic modelling approach in Baklouti et al. (2006). In practice, both the growth and uptake rates are regulated by dimensionless coefficients, respectively, f_Q for primary production and f_Q^{upt} for net uptake, which are functions of the nutrient quota $Q = \text{N/C}$. (see Eqs. (14) and (20)–(22)). Since the early work of Droop (1968), several authors have proposed different formulations for f_Q (e.g. Caperon and Meyer, 1972; Geider et al., 1998; Flynn, 2001) and f_Q^{upt} (e.g. Lehman et al., 1975; Geider et al., 1998; Flynn, 2003). Some of them are summarized in Tables 6 and 7, respectively. Our phytoplankton model described in system (14) uses the Droop (1968) formulation for f_Q and that of Lehman et al. (1975) for f_Q^{upt} . The present section is then intended to assess the consequence of that choice for the model outputs by comparing the reference simulation with simulations produced by other formulations of f_Q and f_Q^{upt} .

Table 3
Parameter values

Process	Parameter	Units	Typical range of values	Reference
Uptake	K_N	(mol N) m ⁻³	10 ⁻³ 0.2 × 10 ⁻³ –2.5 × 10 ⁻³ 0.5 × 10 ⁻³	Geider et al. (1998) Druon and Le Fèvre (1999) Van den Meersche et al. (2004)
	K_{DON}	(mol N) m ⁻³	0.19 × 10 ⁻³ –15 × 10 ⁻³ 0.2 × 10 ⁻³ –0.6 × 10 ⁻³	Présing et al. (2000) Chang et al. (1995)
	K_I	(mol N) m ⁻³	7 × 10 ⁻⁶ –1.07 × 10 ⁻³	Harrison et al. (1996)
	I_m	–	0.44–1	Harrison et al. (1996)
	Q_{min}	(mol N) (mol C) ⁻¹	0.034	Geider et al. (1998, 2005)
	Q_{max}	(mol N) (mol C) ⁻¹	0.05	Van den Meersche et al. (2004)
			0.14–0.17	Geider et al. (1998)
0.17 0.15			Van den Meersche et al. (2004) Christian (2005)	
Chlorophyll synthesis	θ_m^N	g Chl (mol N) ⁻¹	2.3–3.4	Moore et al. (2004)
			4.2–5.6	Geider et al. (1998)
			2	Van den Meersche et al. (2004)
Respiration	r_g	(mol C) (mol C) ⁻¹	0.25	Thornley and Cannell (2000)
	r_{u,NO_3}	(mol C) (mol N uptake) ⁻¹	0.397	Thornley and Cannell (2000)
	$r_{u,N}$	(mol C) (mol N uptake) ⁻¹	0.198	Thornley and Cannell (2000)
	r_{r,NO_3}	(mol C) (mol N reduced) ⁻¹	1.98	Thornley and Cannell (2000)
Remineralization	R_{rem}	s ⁻¹	0.11 × 10 ⁻⁶ 0.003 × 10 ⁻⁶ –4.6 × 10 ⁻⁶	Moore et al. (2004) Christian (2005)
			Detritus breakdown	R_{bd}
Mortality	m_p	s ⁻¹		

Table 4
Model parameter nominal values used in simulations unless noted otherwise

Parameter	Symbol	Nominal value	Standard deviation (SD)	Normalized SD (%)
Half-saturation constant for NO ₃ and NH ₄ uptakes	K_N	1.35 × 10 ⁻³	0.6 × 10 ⁻³	44
Half-saturation constant for DON uptake	K_{DON}	7.6 × 10 ⁻³	3.7 × 10 ⁻³	49
Half-saturation inhibition constant	K_I	0.54 × 10 ⁻³	0.26 × 10 ⁻³	49
Maximum realized inhibition ∈ [0;1]	I_m	0.72	0.14	19
Minimum nitrogen:carbon ratio	Q_{min}	0.042	0.004	10
Maximum nitrogen:carbon ratio	Q_{max}	0.155	0.008	5
Maximum chlorophyll:nitrogen ratio	θ_m^N	3.8	0.9	24
Respiration cost for growth	r_g	0.25	0.06	24
Respiration cost for nitrate uptake	r_{u,NO_3}	0.397	0.1	25
Respiration cost for ammonium and DON uptakes	$r_{u,N}$	0.198	0.05	25
Respiration cost for nitrate reduction	r_{r,NO_3}	1.98	0.5	25
DON remineralization rate	R_{rem}	2.3 × 10 ⁻⁶	1.15 × 10 ⁻⁶	50
Detritus breakdown rate	R_{bd}	0.8 × 10 ⁻⁶	0.1 × 10 ⁻⁶	14
Phytoplankton mortality	m_p	0.8 × 10 ⁻⁶	0.2 × 10 ⁻⁶	27

Parameter units are given in Table 3.

In Fig. 6a functions f_{Q2} and f_{Q4} are normalized (i.e. $f_Q \in [0;1]$) when Q is in the range $[Q_{min}; Q_{max}]$, while this is not true for f_{Q1} and f_{Q3} for which the value at Q_{max} depends on the Q_{min} and K_Q parameters, respectively. The f_{Q1} formulation has the great advantage of involving only a single parameter, though it is less flexible than

Table 5
Initial values for state variables and for Q and θ ratios

Symbol	Nature	Value	Units
C	Phytoplankton carbon	1.3×10^{-3}	mol C m ⁻³
N	Phytoplankton nitrogen	0.19×10^{-3}	mol N m ⁻³
Chl	Phytoplankton chlorophyll	0.325×10^{-3}	g Chl m ⁻³
NO ₃	Nitrate	0.1×10^{-3}	mol N m ⁻³
NH ₄	Ammonium	0.1×10^{-3}	mol N m ⁻³
DON	Dissolved organic nitrogen	0	mol N m ⁻³
PON	Detrital nitrogen	0	mol N m ⁻³
Q	N:C ratio	0.146	mol N (mol C) ⁻¹
θ	Chl:C ratio	0.25	g Chl (mol C) ⁻¹

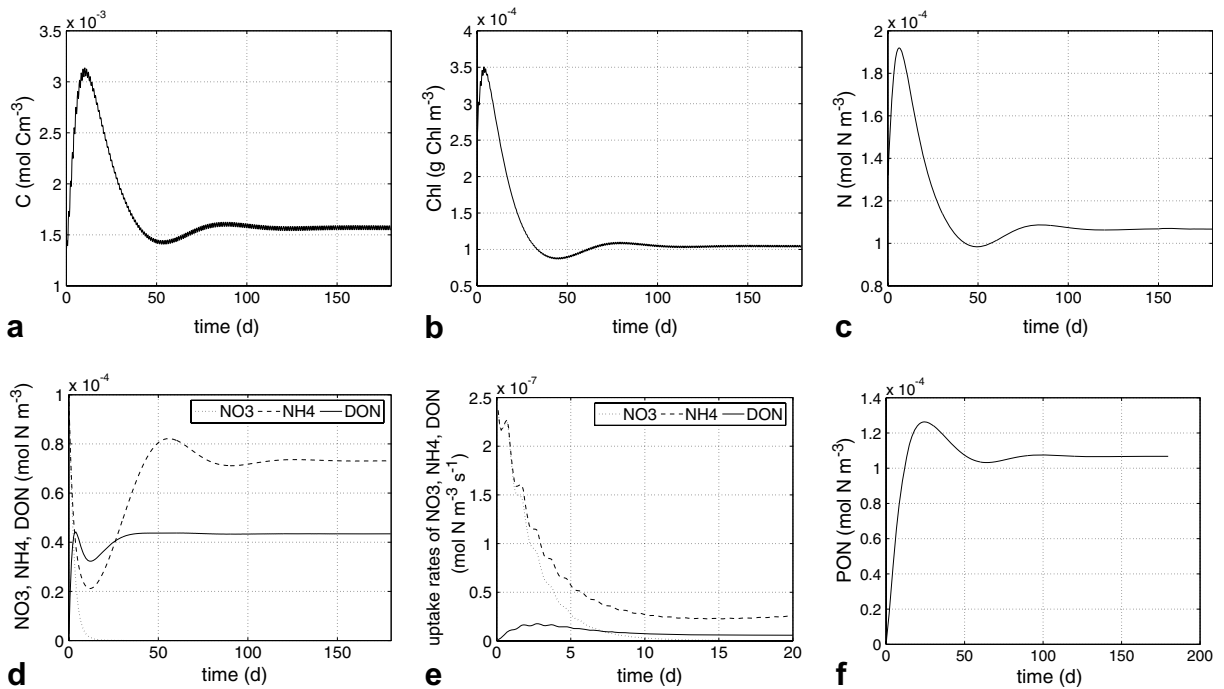


Fig. 5. Outputs of the reference simulation: (a) carbon, (b) chlorophyll, (c) nitrogen phytoplankton internal concentrations, (d) nitrate, ammonium and DON concentrations, (e) nitrate, ammonium and DON uptake rates, (f) PON concentration.

Table 6

Usual functions for quota models. In expressions (2) and (4), K_Q is a quota curvature constant. These functions are plotted in Fig. 6a

f_Q	Reference
$f_{Q1} = \frac{Q - Q_{\min}}{Q}$	Droop (1968)
$f_{Q2} = \frac{Q - Q_{\min}}{Q - Q_{\min} + K_Q}$	Caperon and Meyer (1972)
$f_{Q3} = \frac{Q - Q_{\min}}{Q_{\max} - Q_{\min}}$	Geider et al. (1998)
$f_{Q4} = \frac{(1 + K_Q) \cdot (Q - Q_{\min})}{Q - Q_{\min} + K_Q \cdot (Q_{\max} - Q_{\min})}$	Flynn (2003)

f_{Q2} and f_{Q4} for representing different shapes of curves. For example, Flynn (2003) suggests that parameter K_Q in f_{Q4} should be greater than 0.5 for a typical N quota curve, while for phosphate, this parameter is typically low (<0.2).

Table 7
Example of functions f_Q^{upt} for quota models

f_Q^{upt}	Reference
$f_{Q1}^{\text{upt}} = \frac{Q_{\text{max}} - Q}{Q_{\text{max}} - Q_{\text{min}}}$	Lehman et al. (1975)
$f_{Q2}^{\text{upt}} = \left(\frac{Q_{\text{max}} - Q}{Q_{\text{max}} - Q_{\text{min}}}\right)^n$	Geider et al. (1998)
$f_{Q3}^{\text{upt}} = \frac{1 - Q/Q_{\text{max}}}{1 - Q/Q_{\text{max}} + K_Q}$	Flynn (2003)

In expression (3), K_Q is a quota curvature constant. These functions are plotted in Fig. 6b.

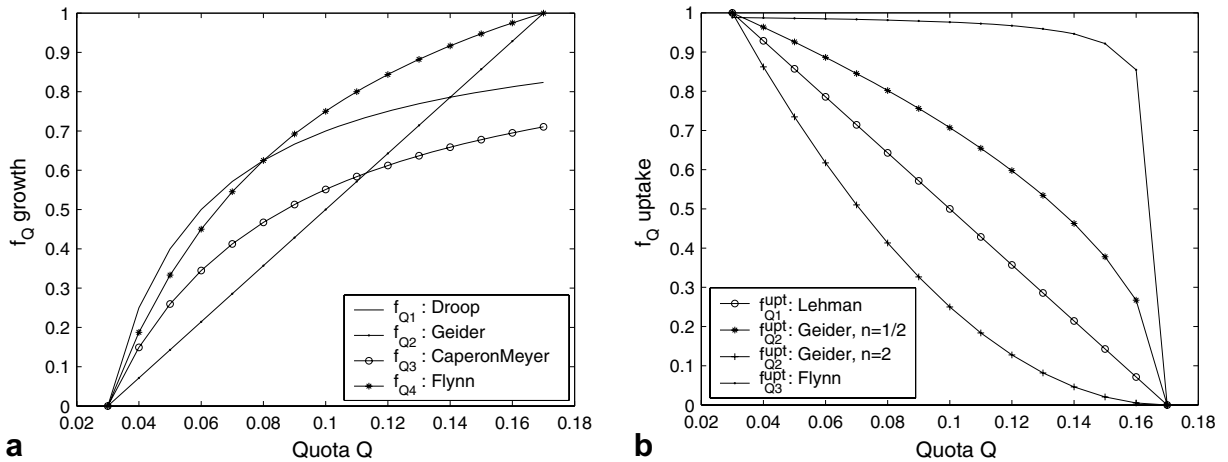


Fig. 6. (a) f_Q (growth) as a function of quota Q . For Caperon–Meyer, $K_Q = 0.057$; for Flynn, $K_Q = 0.5$. $Q_{\text{min}} = 0.03$ and $Q_{\text{max}} = 0.17$. (b) f_Q^{upt} (uptake) as a function of quota Q . For f_{Q3}^{upt} , $K_Q = 0.01$.

With the exception of f_{Q3}^{upt} , the f_Q^{upt} functions are bounded by 0 and 1 in the range $[Q_{\text{min}}; Q_{\text{max}}]$, independently of the parameter values (see Fig. 6b). The abrupt shape of f_{Q3}^{upt} infers that nutrient uptake is almost maximum until Q reaches Q_{max} , whereas for f_{Q1}^{upt} and f_{Q2}^{upt} , the uptake rate decreases as soon as Q rises above Q_{min} .

The choice of the Droop (1968) formulation (f_{Q1}) for f_Q and of the Lehman et al. (1975) one (f_{Q1}^{upt}) for f_Q^{upt} for the present phytoplankton model is above all based on simplicity (both these formulations involve the fewest parameters), since none of the quota functions rely on a merely mechanistic basis (otherwise the mechanistic formulation would have been selected). In order to assess the consequences of our choice, simulations involving other quota function have been undertaken. These simulations solve the same equations as in system (14), with the exception of the quota functions that are different, using the same parameters and initial conditions as in the reference simulation. Corresponding outputs are presented in Figs. 7a–c for the tests relative to f_Q and in Figs. 7d–f for those relative to f_Q^{upt} . To study the growth quota function (f_Q) effect, f_Q^{upt} is set to f_{Q1}^{upt} , and f_Q is set to f_{Q1} when f_Q^{upt} is varied.

Though it is quite reassuring to see that similar patterns of carbon, N:C and Chl:C are observed for all the f_Q and f_Q^{upt} formulations (see Figs. 7a–c), significant quantitative differences do arise from use of different f_Q quota functions. The Flynn (2003) (Geider et al., 1998) expressions predict the highest (lowest) carbon concentrations and, therefore, the minimum (maximum) N:C and Chl:C ratios. The maximum phytoplanktonic C concentration occurs with a maximum time shift of one day between the different formulations, and the carbon concentration is up to 35% higher with f_{Q4} than with f_{Q2} (see Fig. 7a). Moreover, the relative errors of intracellular quotas between the two latter formulations are less than 22.5% and 22%, respectively, for the N:C and Chl:C quotas (see Fig. 7b). The f_{Q3}^{upt} formulation (see Figs. 7d–f) has much less effect on the biomass dynamics (less than 5%, 7% and 6% relative change, respectively, for carbon, N:C and Chl:C among the different quota functions).

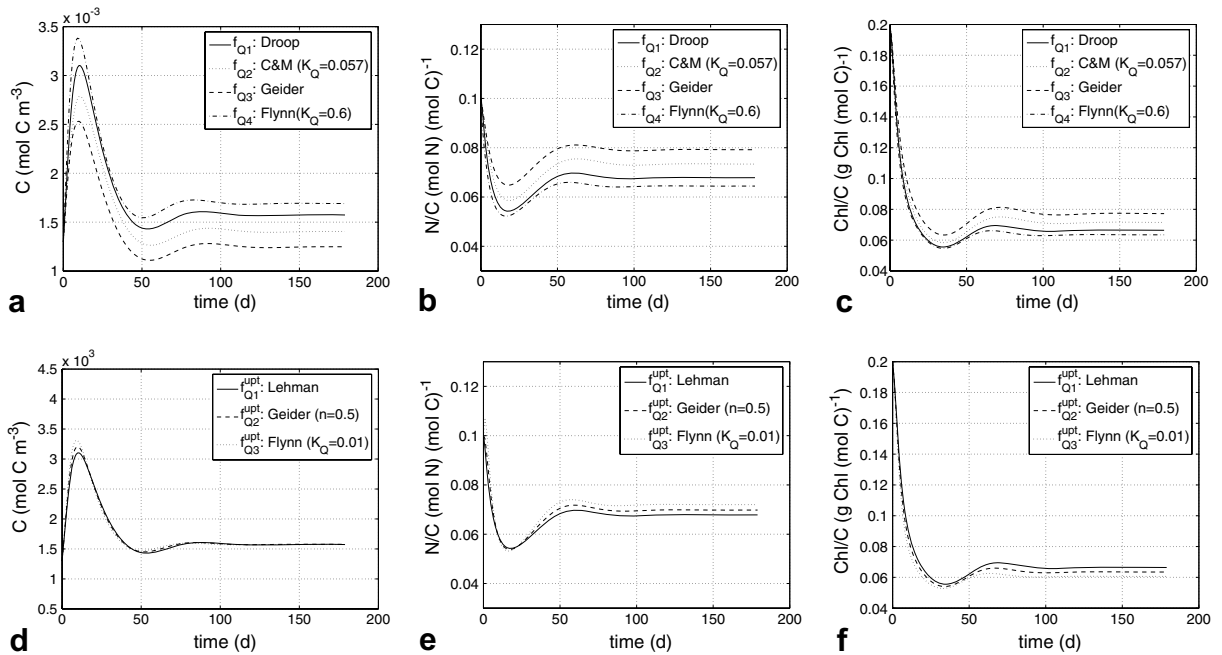


Fig. 7. Top: simulation outputs for the different growth quota formulations (f_Q) reported in Table 6 with function f_Q^{upt} set to the Lehman et al. (1975) expression: (a) phytoplanktonic carbon C, (b) nitrogen:carbon ratio N:C, (c) chlorophyll:carbon ratio Chl:C. Bottom: (d)–(f) represent the same outputs as in (a)–(c), respectively, but for the different nutrient uptake quota formulations (f_Q^{upt}) reported in Table 7 and for f_Q set to the Droop (1968) expression.

Hence, although the global dynamics of the model are not altered by the shape of the quota function, significant differences can arise in the model output values, especially with different f_Q quota functions. As already mentioned, our model uses the Droop (1968) (i.e. f_{Q1}) function giving intermediate results between the Geider et al. (1998) and Flynn (2003) ones, and the linear expression from Lehman et al. (1975) for f_Q^{upt} that confers slight differences from the other expressions. This a priori selection ultimately proved to be very acceptable, though further improvement of the model could include nutrient-specific quota functions.

4.3. Model sensitivity analysis

Significant variations of biogeochemical parameters are depicted in the literature, and this led us to apply a global rather than a local sensitivity analysis. For this, we used a Monte Carlo method, the most widely used technique for global SA (Balakrishnan et al., 2005). Given input probability distributions of the model parameters, Monte Carlo methods involve successive generation of parameter samples followed by application of the model to these samples to yield a set of model responses. These model outputs can then be analyzed statistically giving the resulting uncertainty for some key features (e.g. primary production rate).

The sensitivity analysis evaluates the propagation of input parameter variation through the model and how this influences various model outputs (e.g. primary production rate). The standard deviation of a given simulation output is a measure of uncertainty (derived from the input variation/uncertainty), and at the same time, a measure of the sensitivity of this output with respect to an/the input parameter(s). The uncertainty will be the range in which the output variable is distributed, caused by the distribution of the input parameter(s). The sensitivity is given by the spread of the output distribution in relation to the spread of input distribution. A wide distribution in the output caused by a low width in the input would suggest a high sensitivity of the model to the parameter under study. The effects of one-at-a-time parameter deviations were investigated first for our model that involves $n_p = 20$ parameters $(p_i)_{1 \leq i \leq n_p}$. Twenty simulations of 180 days duration ($t_f = 180$ days) were conducted for which only one parameter at a time was perturbed while the others were fixed to

their nominal values given in Tables 2 and 4. For each simulation, the varying parameter took N random values from a normal distribution centered at the parameter nominal value, and probability distributions for outputs were generated. In order to compare the individual effect of each parameter, an identical normalized standard deviation of 25 % was associated with each parameter's normal distribution. A second analysis was also performed in which the standard deviations of the input distributions were parameter-specific and took their respective values reported in Tables 2 and 4. Actually, both analyses seemed relevant to us: The first is often encountered in the literature and provides insight regarding the sensitivity of the simulation outputs to the model parameters, given identical relative uncertainties of the parameters. This allows determination of which parameters are the most influential for the numerical solution. By contrast, the use of realistic ranges of variation for each parameter is more relevant to test the range of the model outputs given the actual spread of a given parameter (Druon and Le Fèvre, 1999). The simulation outputs investigated were the carbon-specific primary production rate P^C , the carbon concentration C , the phytoplankton Chl:C ratio θ and the phytoplankton N:C ratio Q . Each of these outputs was averaged over the simulation duration (180 days) and in what follows, every mention in the text of simulation outputs implicitly refers to the corresponding averaged outputs over the simulation duration. Except for the reference simulation, for which all the parameters were fixed to their nominal values, the present analysis varied the parameter under concern through a simulation of N runs. The required number of samples (N) is a function of model complexity. In general, the greater the number of model parameters, the greater the number of samples required before model outputs stabilize. The simulation illustrated here stabilized at around 3000 samples, as shown in Fig. 8 where the mean values of the carbon-specific production rate and the phytoplanktonic carbon concentration are reported as functions of the number of Monte Carlo samples. In what follows N value was therefore set to 4000.

The sensitivity results are reported in Fig. 9 for identical normalized standard deviations for the whole set of the input parameters tested one at a time. Each output distribution roughly follows a normal distribution, the mean of which is approximately equal to the corresponding output value provided by the reference simulation. Normalized standard deviations (Fig. 9) have been calculated for each output distribution derived from each varying parameter. Clearly, the most influential parameter(s) differ depending on the output under consideration. For example, the carbon specific primary production rate, P^C , is mostly influenced by three parameters: the respiration cost for growth (r_g), the maximum N:C ratio (Q_{\max}) and the mortality rate (m_p), albeit the first two exert moderate influences (less than 10% for input standard deviations of 25%). The specific mortality rate, however, has a significant effect on P^C ($s(P^C) = 22\%$). As expected, parameters \bar{a}^* and ϕ_m^C were found to have identical effects on P^* (and on the remaining outputs as well), since they have similar roles in the model (see Eq. (16)) and since the normalized standard deviations of both parameter distributions were the same. By contrast, eight parameters generated phytoplankton carbon C normalized standard deviations higher than 10%, among which Q_{\min} and m_p were the most influential ($s(C) > 25\%$). Hence,

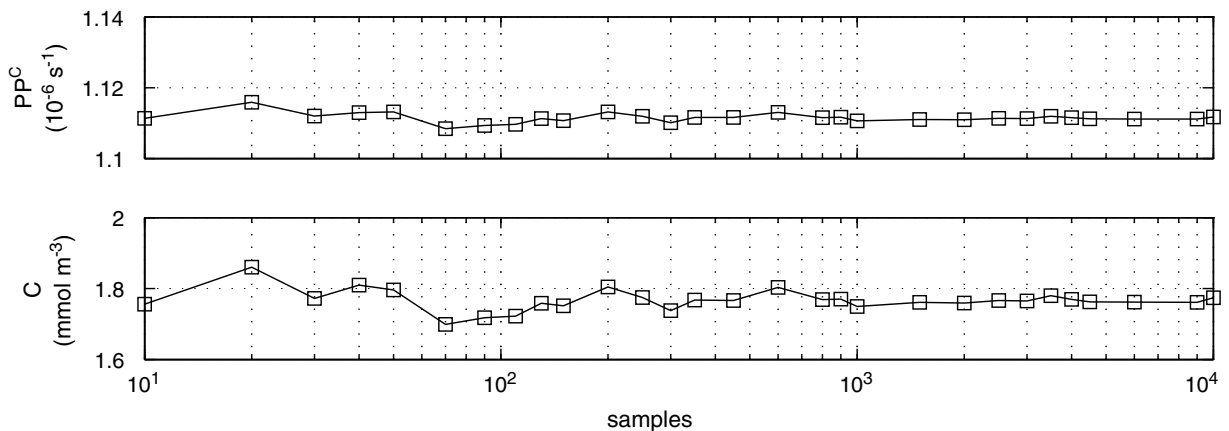


Fig. 8. Mean specific primary production rate (top) and mean phytoplankton carbon concentration (bottom) as functions of the number of Monte Carlo samples, showing stability after about 3000 samples.

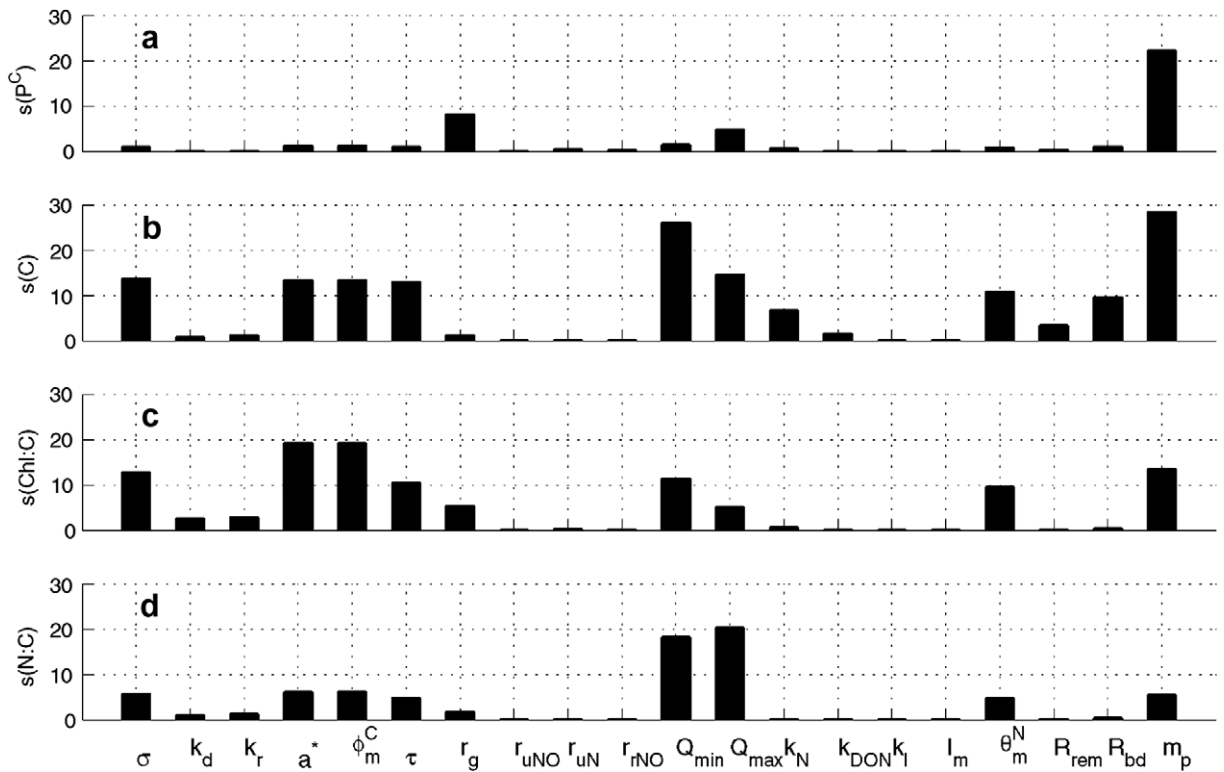


Fig. 9. Sensitivity analysis results for one-at-a-time parameter perturbations with an identical normalized standard deviation for all the input parameter distributions. The normalized standard deviations (in %) of the simulation output distributions are reported here for four outputs, namely (a) the carbon-specific primary production rate P^C , (b) the carbon concentration C , (c) the phytoplankton Chl:C ratio, (d) the phytoplankton N:C ratio. r_{uNO} stands for r_{u,NO_3} and r_{rNO} stands for r_{r,NO_3} .

phytoplankton concentration is much more sensitive than the primary production rate to the model parameters. The dominant influence of m_p on both P^C and C is not surprising, since model closure terms are well-known for the large uncertainties that they produce in model outputs (e.g. [Fulton et al., 2003](#), and references therein).

From [Fig. 9c](#), it appears that the photosynthetic parameters, and especially \bar{a}^* and ϕ_m^C significantly influence the phytoplankton chlorophyll:carbon ratio, with standard deviations around 20%. At last, only the maximum and minimum N:C ratios (respectively Q_{max} and Q_{min}) had significant effects on the phytoplankton N:C ratio ([Fig. 9d](#)).

Sensitivity results differ if we account for the actual variability of parameters through parameter-specific standard deviations (see [Fig. 10](#)). Indeed, some parameters which could be highly influential regarding their implication in the model proved to be only moderately influential parameters since their actual variability is weak. This is typically the case for Q_{min} . By contrast, parameters such as ϕ_m^C turned out to be very highly influential for the four model outputs investigated. Hence, the differences between [Figs. 9 and 10](#) point out that both sensitivity analyses are useful and provide different information: the first SA, which uses equal normalized standard deviations ([Fig. 9](#)), allows comparison of the respective influences of model parameters when they are all characterized by the same relative uncertainty, while the second SA ([Fig. 10](#)) informs about their effective influence accounting for their actual uncertainty. As a matter of fact, the use of arbitrary fixed standard deviations for the input parameters does not reflect the actual influence on the outputs, which is highlighted by the comparison of [Figs. 9 and 10](#).

Finally, output uncertainties are reported in [Fig. 11](#) for specific parameter distributions. In this figure, the output ranges associated with each varying parameter are plotted, as well as the output value provided by the reference simulation (dotted line). For each varying parameter the mean of the output distribution is repre-

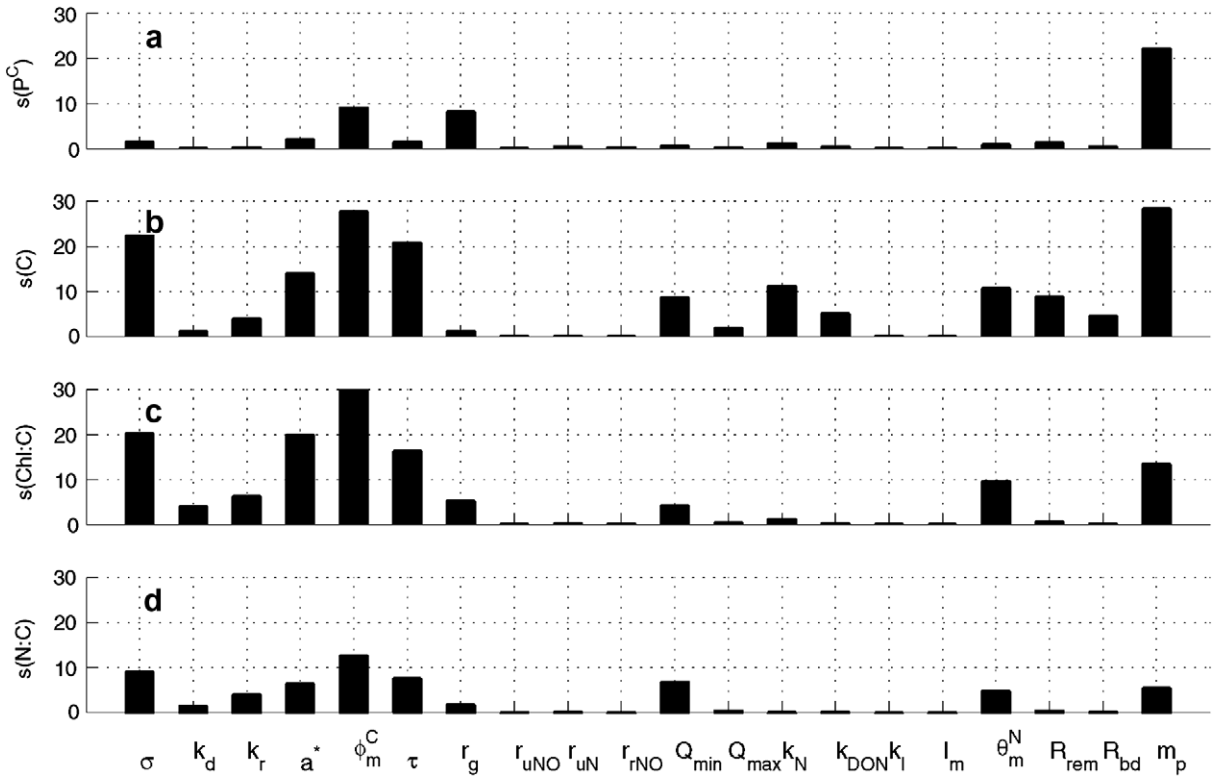


Fig. 10. Identical to Fig. 9 but with parameter-specific normalized standard deviations for the input distributions.

sented by a square marker. This figure also reports the output range provided by simultaneous parameter perturbations. Simultaneous perturbation analyses have seldom been undertaken so far for ecosystem models, though they provide important information relative to the actual uncertainty of the model outputs. As a matter of fact, the cumulative effect of the parameter uncertainties on the simulation outputs cannot be estimated from the effects of individual parameter perturbations. From Fig. 11 it can only be said that the simultaneous perturbations always generate a higher output spread than the most influential parameter (i.e. the one that brings out the highest standard deviation for the output distribution when it alone is perturbed). The output distribution standard deviation resulting from the simultaneous parameter deviations is also unpredictable from the magnitudes of the standard deviations obtained by the one parameter at a time analyses, at least for non-linear models. Instead, many situations may arise from simultaneous parameter perturbations where the effects of interactions between parameters can either partially moderate their individual effects or produce a joint effect greater than the sum of the individual effects. Hence, although it is scarcely possible to reduce the input parameter uncertainties, it is at least possible to estimate the effect of these uncertainties on the model outputs and to assess the level of confidence that can be put in them. This can be undertaken even for more complex, computationally burdensome models with specific uncertainty analysis techniques like the stochastic response surface method (SRSM) or the high dimensional model representation (HDMR) that reduce the number of model simulations required for adequate estimation of uncertainty. These methods provide results that are practically indistinguishable from those obtained using conventional Monte Carlo methods, while requiring orders of magnitude fewer model simulations (Balakrishnan et al., 2005).

4.4. Model comparison with chemostat experiments

Comparison of model outputs with experiments is an additional essential step in modelling. The validation procedure we focus on here is the dynamic behavior of our model with regard to three chemostat experiments. The latter were performed on the marine diatom *Thalassiosira weissflogii* by Pawlowski (2004) to investigate

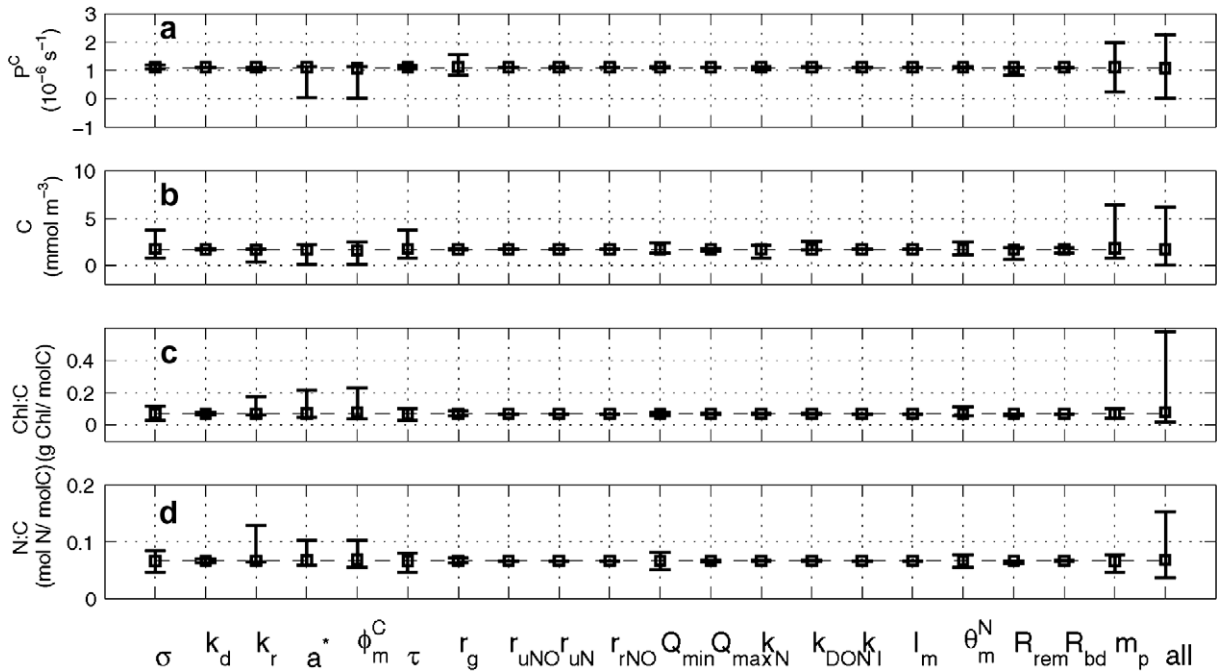


Fig. 11. Sensitivity analysis results for one-at-a-time and simultaneous (label 'all' in the x -axis) parameter perturbations with parameter-specific standard deviation for the input parameter distributions. The simulation output ranges are reported here for four outputs, namely (a) the carbon-specific primary production rate P^C , (b) the carbon concentration C , (c) the phytoplankton Chl:C ratio, (d) the phytoplankton N:C ratio.

the effect of simultaneous limitations by light and nutrient availability on algal growth. During four days, algae grew up in batch conditions and were submitted to a constant light intensity ($E = 250 \mu\text{mol quanta m}^{-2} \text{s}^{-1}$). This adaptation period was followed by the activation of a light/dark cycle and by a switch into continuous culture mode. Diatom cultures were NO_3^- -limited and submitted to either low light (LL) cycles of $180 \mu\text{mol quanta m}^{-2} \text{s}^{-1}$ maximum irradiance for one culture or to high light (HL) cycles of $850 \mu\text{mol quanta m}^{-2} \text{s}^{-1}$ maximum irradiance in the two remaining chemostats (duplicates HL1 and HL2). Twenty-four days after the beginning of the experiment, light cycles were stopped and replaced by a constant irradiation of 100 and $400 \mu\text{mol quanta m}^{-2} \text{s}^{-1}$, respectively, for the LL and HL cultures. Using the same dilution rate (0.4 d^{-1}), light variations with time, inflow nitrate concentration and initial conditions as in the experimental setup, we have simulated the culture behavior in open reactor mode. The model used is the same as in system (14) apart from removal of the NH_4 and the detrital compartments and zeroing of the remineralization and natural mortality processes (R_{rem} and m_p were set to zero). To insure mass conservation, additional terms relative to the water outflow from the chemostat were added in Eqs. (14b)–(14e). Then the nitrate conservation equation (Eq. (14e)) was completed with an additional inflow term. The three chemostats were stirred so that we assume the water volume is homogenous.

Comparisons of the simulations with the culture experiments are given in Figs. 12 and 13 for the LL and the HL experiments, respectively (only one HL experiment has been considered as both give similar results). Experimental data were available only 20 days after the beginning of the experiment. Simulations have been performed with the parameter values given in Table 8. The latter were derived from the literature and were mostly from *T. weissflogii* experiments. The remaining parameters were set to their nominal values given in Tables 2 and 4, with the exception of the average chlorophyll-specific absorption coefficient (\bar{a}^*) that was tuned to fit the LL experiment. It must be noted that the value ultimately used for \bar{a}^* still belongs to the range of values reported in Table 1 for this parameter. Moreover, our aim was obviously not to find the best set of parameters, but rather to use realistic parameter values and to test our model's ability to represent phytoplankton dynamics in two different light regimes using the same parameter values for both.

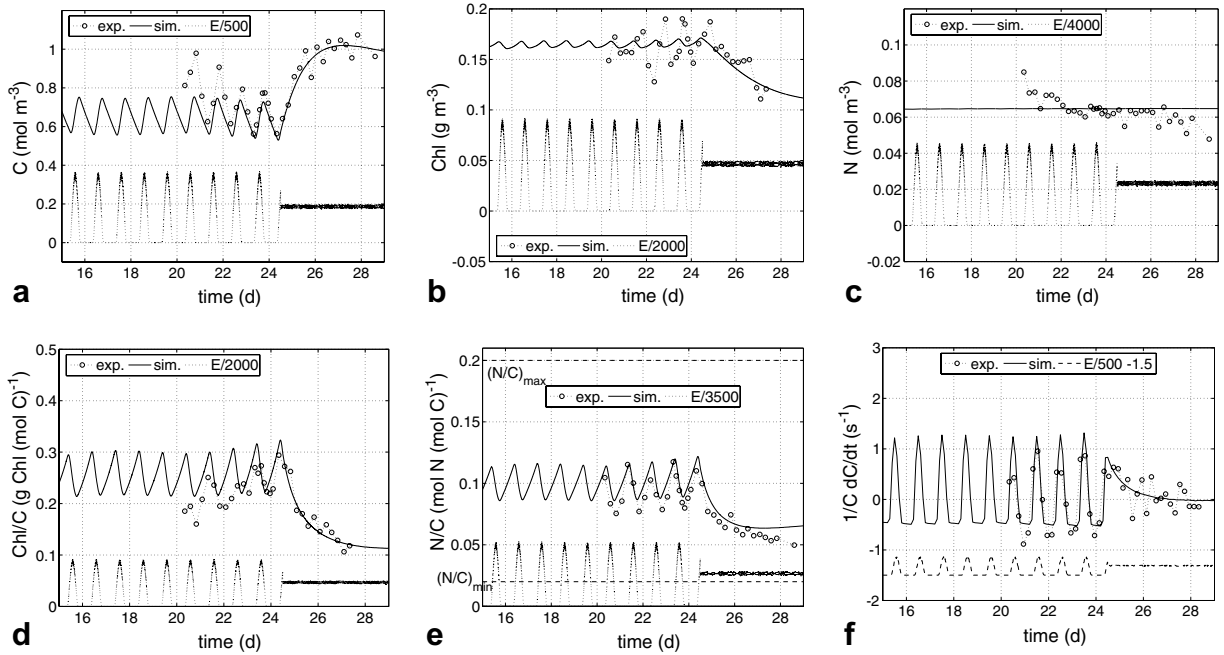


Fig. 12. Comparison of a chemostat experiment (open circles, Pawlowski, 2004) with simulation outputs under low light conditions (LL): (a) phytoplankton carbon C, (b) phytoplankton chlorophyll Chl, (c) phytoplankton nitrogen N, (d) phytoplankton chlorophyll:carbon ratio, (e) nitrogen:carbon intracellular ratio and (f) specific growth rate $\mu = \frac{1}{C} \frac{dC}{dt}$. E refers to the measured irradiance in $\mu\text{mol quanta m}^{-2} \text{s}^{-1}$.

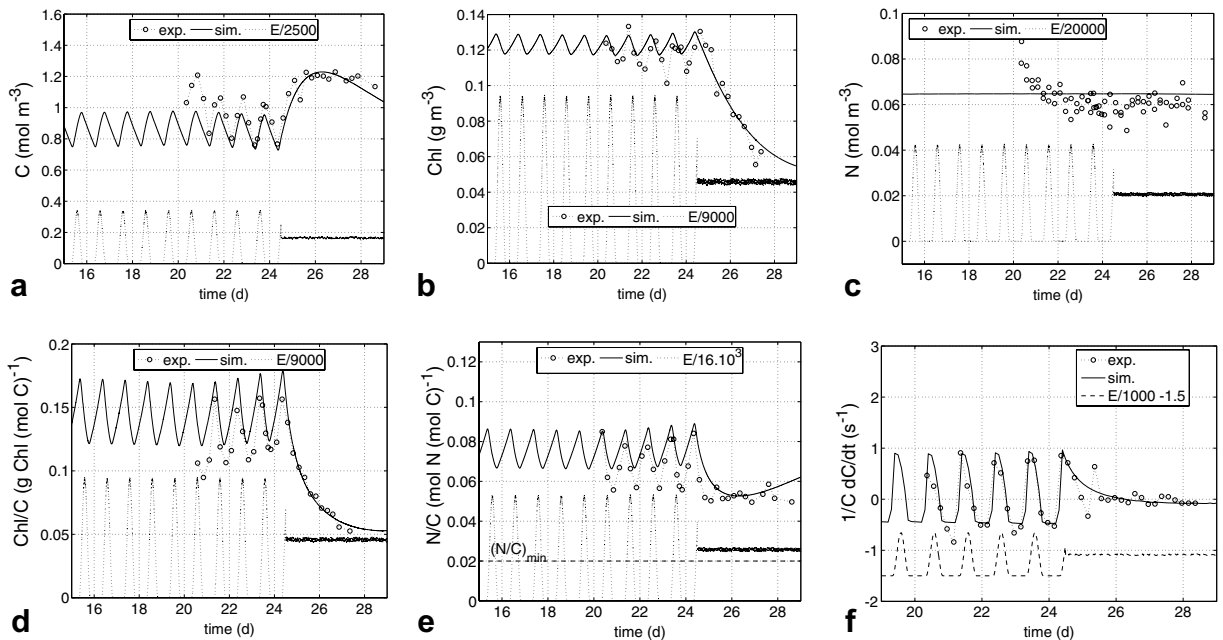


Fig. 13. Comparison of a chemostat experiment (open circles, Pawlowski, 2004) with simulation outputs under high light conditions (HL): (a) phytoplankton carbon C, (b) phytoplankton chlorophyll Chl, (c) phytoplankton nitrogen N, (d) phytoplankton chlorophyll:carbon ratio, (e) nitrogen:carbon intracellular ratio and (f) specific growth rate $\mu = \frac{1}{C} \frac{dC}{dt}$. E refers to the measured irradiance in $\mu\text{mol quanta m}^{-2} \text{s}^{-1}$.

Table 8
Parameter values used for model comparison with chemostat experiments

Parameter	Value	Units	Reference
\bar{a}^*	41	$\text{m}^2 (\text{g}; \text{Chl})^{-1}$	Tuned
k_d^H	3.5×10^{-8}	–	Nominal value from Table 2
k_r	1.6×10^{-4}	s^{-1}	Nominal value from Table 2
ϕ_m^C	0.035^a	$(\text{mol C}) (\text{mol quanta})^{-1}$	Finkel (2001)
σ	307^b	$\text{\AA}^2 \text{ quanta}^{-1}$	Suggett et al. (2004)
τ	2.8×10^{-3c}	s	Behrenfeld et al. (1998)
K_N	2.5×10^{-3d}	$(\text{mol N}) \text{m}^{-3}$	Moore et al. (2004)
Q_{\min}	0.02^e	$(\text{mol N}) (\text{mol C})^{-1}$	Finkel (2005)
Q_{\max}	0.2^f	$(\text{mol N}) (\text{mol C})^{-1}$	Pawlowski (2004)
θ_m^N	2.9^f	$\text{g Chl} (\text{mol N})^{-1}$	Pawlowski (2004)
r_g	0.25	$(\text{mol C}) (\text{mol C})^{-1}$	Nominal value from Table 4
$r_{u,N}$	0.397	$(\text{mol C}) (\text{mol N uptake})^{-1}$	Nominal value from Table 4
$r_{u,DON}$	0.198	$(\text{mol C}) (\text{mol N uptake})^{-1}$	Nominal value from Table 4
r_{rN}	1.98	$(\text{mol C}) (\text{mol N reduced})^{-1}$	Nominal value form Table 4

Most of these values are specific to *Thalassiosira weissflogii*. Others values are taken from Tables 2 and 4 or from steady-state experiments performed on *T. weissflogii* (see Pawlowski (2004)) while the average Chla-specific absorption coefficient has been tuned.

^a This value is calculated by the relation $\phi_m^C = aV^b$ where V is the cells volume determined with an equivalent diameter of $12.5 \mu\text{m}$ (in Pawlowski (2004), the equivalent diameter of the culture of *T. weissflogii* is in the range $10\text{--}15 \mu\text{m}$) and coefficients have been estimated to $a = 0.0769$ and $b = -0.11$ from Fig. 5 in Finkel (2001).

^b Mean value for *T. weissflogii*.

^c Determined from Fig. 3 in Behrenfeld et al. (1998) from experiments on *T. weissflogii*. This value corresponds to an irradiance of $515 \mu\text{mol quanta m}^{-2} \text{s}^{-1}$ which is the mean irradiance of the LL and HL chemostat experiments.

^d Value given for diatoms in Moore et al. (2004).

^e Calculated with the relation $Q_{\min} = aV^b$, where V is the cells' volume. Coefficients $a = 1.5 \times 10^{-9}$ and $b = 1.92 \times 10^{-7}$ are given in Finkel (2005). The relation provides a value of Q_{\min} in $\mu\text{mol N}$ per cell which was converted in $(\text{mol N})/(\text{mol C})$. The corresponding conversion factor was set to $130 \times 10^{-12} \text{gC/cell}$, which is the mean value determined from Pawlowski's (2004) experiments.

^f From steady-state experiments on *T. weissflogii* presented in Pawlowski (2004).

Figs. 12 and 13 compare chemostat data with simulation outputs for the LL and the HL cases. They indicate a good fit between observed and predicted outputs, not only for phytoplankton carbon and chlorophyll but for the intracellular ratios. These figures illustrate the ability of our model in representing phytoplankton dynamics and stoichiometry variations. Except for nitrogen, the simulated cyclic fluctuations induced by the light-dark cycles are in phase with and about of the same amplitude as the measured ones. Though simulated chlorophyll concentrations are closely consistent with measurements, the amplitude of the chlorophyll cycles were slightly underestimated by the model, and the peaks were slightly shifted back. This is clearly due to the fact that chlorophyll synthesis is enabled in darkness by the model, and future improvement could include a restriction of Chl synthesis at night. No periodicity of measured nitrogen concentrations reflecting the length of the photoperiod was evident upon examination of Figs. 12 and 13c. Instead, N is relatively constant during the light-dark cycles, at least between the 22nd and 27th days, and the corresponding values are in good agreement with model predictions. At the end of the LL experiment, a decrease in the N concentration, the origin of which is unknown (all the more uncertain because this was not observed in the HL experiment), made the $N:C$ data ultimately deviate from the simulated curve (see Fig. 12e). Moreover, the simulated carbon concentration in the HL case is slightly underestimated, contrary to chlorophyll which is slightly overestimated. Consequently, the simulated Chl:C ratio in the HL case is slightly overestimated, though the amplitude of its variations are consistent with measured Chl:C . This could be due to the fact that in our model, the absorption cross-section (σ) and the turnover time of the electron transport chain (τ) are not modified by the Chl:C ratio which is affected by photoacclimation. The carbon specific growth rate $\mu = \frac{1}{C} \cdot \frac{dC}{dt}$ has been represented in Fig. 12d, showing that the maxima in μ coincide with the maxima in light cycles and, therefore, that no photoinhibition occurs. As expected, the maxima in C are slightly shifted back and arise about four hours after the light maxima when irradiance shifts to a constant value, biomass oscillations stop and phytoplankton carbon increases until intracellular nutrient reserves are exhausted (Q near Q_{\min}), after which carbon and especially chlorophyll concentrations decrease dramatically. These tendencies are, again, well reproduced by the model for the phytoplankton carbon and chlorophyll.

The latter results demonstrate that many important features of photoacclimation are captured by the present model. First, it reproduced the 2-fold decrease observed in the Chl:C ratio with increasing irradiance, without modifying parameter values (around 0.12 g Chl (mol C)⁻¹ in the LL case against 0.06 in the HL one at the end of the experiment). Moreover, the decrease in the Chl:N ratio between the LL and HL simulations conveys the fact that the part of the assimilated nitrogen dedicated to the synthesis of photosynthetic pigments decreases as light becomes less limiting (in comparison with nitrogen).

The present model accounts not only for the change in stoichiometry induced by photoacclimation, but it also includes the subsequent change in the P vs E curve through parallel changes in the chlorophyll-specific initial slope α^* (see Eq. (27)) and the maximum chlorophyll-specific primary production rate P_{\max}^* , both of which are consistent with the frequently observed positive correlation between the light-limited slope and the light-saturated rate of photosynthesis (Behrenfeld et al., 2004)

$$\alpha^* = \bar{\alpha}^* \cdot \phi^C = \bar{\alpha}^* \cdot \phi_m^C \cdot n_o. \quad (27)$$

In our model, α^* varies with the proportion, (n_o), of open PSII. This model is, therefore, able to represent the reductions of α^* that may arise at high irradiance due to reductions in the quantum efficiency of photosynthesis associated with either the accumulation of photoinhibitory damage or reversible down-regulation of exciton transfer from the light-harvesting antennae to the reaction centers (Geider et al., 1997).

In conclusion, though further validation operations should be undertaken, our model gives a satisfactory description of the phytoplankton dynamics submitted to cyclic irradiance under nitrogen-limited conditions. This model also reproduces photoacclimation via a specific mass conservation equation for chlorophyll as formulated in Eq. (14). However, as DON concentrations were not measured in Pawlowski (2004) experiments, the present set of data did not allow us to validate the uptake/exudation model as formulated in system (14). Finally, though the present model is quite simple compared to what actually takes place in natural marine populations, this study can however be considered as a first step toward our aim of achieving realistic modelling of phytoplankton dynamics.

5. Conclusion and perspectives

We have introduced a new modular numerical tool Eco3M dedicated to biogeochemical modelling. It has a great advantage in that the number and the nature of the model state variables, as well as the models for biogeochemical processes, are decided by the user without entering the code sources. Moreover, a numerical library of biogeochemical process models is already available, and any new formulation can be added to it with great simplicity.

Analysis of Eco3M default formulations relative to phytoplankton dynamics has been the purpose of the rest of the paper. The photosynthesis model component relying on Han's (2002) model has been investigated first. In substance, its dynamic and stationary solutions have been compared, and it appears that in presence of rapid light changes as encountered in high light environments or in presence of vertical mixing, the steady-state solution overestimates photosynthesis. On the other hand, substantial complexity is introduced by the use of the dynamic model for which the numerical solution is not trivial. An alternative solution has consisted in reducing the dynamic model to a single equation that can be numerically integrated with simplicity. Computational costs are greatly decreased, which is of great interest for further coupling of the biogeochemical model with a hydrodynamical transport model.

The rest of the paper enlarges the study to evaluation of a dynamic phytoplankton model among the class of models presented in Baklouti et al. (2006) that incorporates some other key phytoplankton processes, namely autotrophic respiration, uptake and exudation. Moreover, bacterial and zooplanktonic activities are implicitly (although simplistically) considered through detritus breakdown, dissolved organic matter remineralization and phytoplankton mortality. Several quota functions associated with uptake and growth have been tested, and the results differed significantly according to the formulation used, especially for the quota function associated with growth. Further use of the present model should involve particular care in the choice of the latter functions, and it is likely that the nature of the nutrient taken up has to be considered in making this choice.

Considering that model testing consists of several steps, one of which should be the determination of which parameters are the most influential on model outputs, a global sensitivity analysis of the phytoplankton model has been carried out using a Monte Carlo method. Our SA combined two different strategies for parameter sampling: (1) assigning equal normalized standard deviations to the whole set of input parameter distributions, and (2) applying parameter-specific input distributions based on a realistic range of values for each parameter. Both strategies are relevant and give different information: the model's sensitivity to its parameters for the former and actual uncertainties of the model outputs for the latter. Sensitivity analysis enabled us to identify the most influential parameters, those that most warrant accurate measurement. The SA also serves as a guide to any further use of the model. Furthermore, the comparison of the SA results provided by one-at-a-time parameter perturbations to those inferred by simultaneous perturbations revealed that output uncertainties can be greatly underestimated with the former.

The comparison of model outputs with experimental data has demonstrated our model's ability to simulate phytoplankton dynamics, though additional validation operations should be undertaken.

Finally, we have intended to give an overview of the step-by-step approach that can be undertaken for a rigorous analysis of the behavior of any dynamic model. Though applied here to a somewhat simple phytoplankton model, it can obviously be transposed to more complex models provided dedicated systematic methods for model reduction are used. In the same way, sensitivity analysis of large models can be undertaken with specific methods which require fewer model simulations than the conventional Monte Carlo methods.

To conclude, we have focussed on testing the phytoplankton model in isolation before elaborating it in an ecosystem model with more realistic bacterial and zooplankton compartments and physical forcing. We look toward developing these other components in future work.

Acknowledgments

The authors are grateful to Prof. J.C. Poggiale and Dr. David Nerini for their time and willingness to provide thoughtful information and insights and for fruitful scientific discussions.

References

- Auger, P., Lett, C., 2003. Integrative biology: linking levels of organization. *C. R. Biologies* 326, 517–522.
- Babin, M. et al., 1996. Nitrogen- and irradiance-dependent variations of the maximum quantum yield of carbon fixation in eutrophic, mesotrophic and oligotrophic marine systems. *Deep Sea Research I* 43 (8), 1241–1272.
- Baird, M.E., Oke, P.R., Suthers, I.M., Middleton, J.H., 2004. A plankton population model with biomechanical descriptions of biological processes in an idealised 2D ocean basin. *Journal of Marine Systems* 50, 199–222.
- Baird, M.E., Walker, S.J., Wallace, B.B., Webster, I.T., Parslow, J.S., 2003. The use of mechanistic descriptions of algal growth and zooplankton grazing in an estuarine eutrophication model. *Estuarine, Coastal and Shelf Science* 56, 685–695.
- Baklouti, M., Diaz, F., Pinazo, C., Faure, V., Queguiner, B., 2006. Investigation of mechanistic formulations depicting phytoplankton dynamics for models of marine pelagic ecosystems. *Progress in Oceanography*.
- Balakrishnan, S., Roy, A., Ierapetritou, M.G., Flach, G.P., Georgopoulos, P.G., 2005. A comparative assessment of efficient uncertainty analysis techniques for environmental fate and transport models: application to the FACT model. *Journal of Hydrology* 307, 204–218.
- Baroli, I., Melis, A., 1996. Photoinhibition and repair in *dumaliella salina* acclimated to different growth irradiances. *Planta* 198, 640–646.
- Behrenfeld, M.J., Prasil, O., Babin, M., Bruyant, F., 2004. In search of a physiological basis for covariations in light-limited and light-saturated photosynthesis. *Journal of Phycology* 40, 4–25.
- Behrenfeld, M.J., Prasil, O., Kolber, Z.S., Babin, M., Falkowski, P.G., 1998. Compensatory changes in photosystem II electron turnover rates protect photosynthesis from inhibition. *Photosynthesis Research* 58, 259–268.
- Caperon, J., Meyer, J., 1972. Nitrogen-limited growth of marine phytoplankton – I. Changes in population characteristics with steady-state growth rate. *Deep-sea Research* 19, 601–618.
- Chang, F.H., Bradford-Grieve, J.M., Vincent, W.F., Woods, P.H., 1995. Nitrogen uptake by the summer size-fractionated phytoplankton assemblages in the Westland, New Zealand, upwelling system. *New Zealand Journal of Marine and Freshwater Research* 29, 147–161.
- Christian, J.R., 2005. Biogeochemical cycling in the oligotrophic ocean: redfield and non-redfield models. *Limnology and Oceanography* 50 (2), 646–657.
- Collos, Y., Gagne, C., Laabir, M., Vaquer, A., Cecchi, P., Souchu, P., 2004. Nitrogenous nutrition of *Alexandrium catenella* (dinophyceae) in cultures and in Thau lagoon, southern France. *Journal of Phycology* 40, 96–103.
- Droop, M.R., 1968. Vitamin B-12 and marine ecology. 4. the kinetics of uptake, growth and inhibition in *monochrysis lutheri*. *Journal of Marine Biology Association of the United Kingdom* 48, 689–733.

- Druon, J.N., Le Fèvre, J., 1999. Sensitivity of a pelagic ecosystem model to variations of process parameters within a realistic range. *Journal of Marine Systems* 19, 1–26.
- Faugeras, B., Lévy, M., Mémery, L., Verron, J., Blum, J., Charpentier, I., 2003. Can biogeochemical fluxes be recovered from nitrate and chlorophyll data? A case study assimilating data in the Northwestern Mediterranean Sea at the JGOFS-DYFAMED station. *Journal of Marine Systems* 40, 1–27.
- Finkel, Z.V., 2001. Light absorption and size scaling of light-limited metabolism in marine diatoms. *Limnology and Oceanography* 46 (1), 86–94.
- Finkel, Z.V., 2005. Physiological basis for environmentally-driven changes in phytoplankton communities. Technical Report, The State University of New Jersey.
- Flynn, K.J., 2001. A mechanistic model for describing dynamic multi-nutrient, light, temperature interactions in phytoplankton. *Journal of Plankton Research* 23 (9), 977–997.
- Flynn, K.J., 2003. Modelling multi-nutrient interactions in phytoplankton; balancing simplicity and realism. *Progress in Oceanography* 56, 249–279.
- Flynn, K.J., Flynn, K., 1998. Release of nitrite by marine dinoflagellates: development of a mathematical simulation. *Marine Biology* 130, 455–470.
- Fulton, E.A., Smith, A.D.M., Johnson, C.R., 2003. Mortality and predation in ecosystem models: is it important how these are expressed? *Ecological Modelling* 169, 157–178.
- Geider, R.J., MacIntyre, H.L., Kana, T.M., 1997. Dynamic model of phytoplankton growth and acclimation: responses of the balanced growth rate and the chlorophyll *a*: Carbon ratio to light, nutrient-limitation and temperature. *Marine Ecology Progress Series* 148, 187–200.
- Geider, R.J., MacIntyre, H.L., Kana, T.M., 1998. A dynamic regulatory model of phytoplanktonic acclimation to light, nutrients, and temperature. *Limnology and Oceanography* 43 (4), 679–694.
- Gorbinov, M.Y., Kolber, Z.S., Falkowski, P.G., 1999. Measuring photosynthetic parameters in individual algal cells by Fast Repetition Rate fluorimetry. *Photosynthesis Research* 62, 141–153.
- Han, B.P., 2002. A mechanistic model of algal photoinhibition induced by photodamage to photosystem-II. *Journal of Theoretical Biology* 214, 519–527.
- Harrison, W.G., Harris, L.R., Irwin, B.D., 1996. The kinetics of nitrogen utilization in the oceanic mixed layer: nitrate and ammonium interactions at nanomolar concentrations. *Limnology and Oceanography* 41 (1), 16–32.
- Heraud, P., Beardall, J., 2000. Changes in chlorophyll fluorescence during exposure of *dunaliella tertiolecta* to uv radiation indicate a dynamic interaction between damage and repair processes. *Photosynthesis Research* 63, 123–134.
- Johnson, Z., Bidigare, R.R., Goericke, R., Marra, J., Trees, C., Barber, R., 2002. Photosynthetic physiology and physicochemical forcing in the Arabian sea, 1995. *Deep Sea Research I* 49, 415–436.
- Kaňa, R., Lazár, D., Prášil, O., Nauš, J., 2002. Experimental and theoretical studies on the excess capacity of photosystem II. *Photosynthesis Research* 72, 271–284.
- Klepper, O., Peters, J.C.H., Van de Kamer, J.P.G., Eilers, P., 1988. The calculation of primary production in an estuary. A model that incorporates the dynamic response of algae, vertical mixing and basin morphology. In: Marani, A. (Ed.), *Advances in Environmental Modelling*. Elsevier, Amsterdam, pp. 373–394.
- Kolber, S.Z., Ondrej, P., Falkowski, P.G., 1998. Measurements of variable chlorophyll fluorescence using fast repetition rate techniques: defining methodology and experimental protocols. *Biochimica et Biophysica Acta* 1367, 88–106.
- Laney, S.R., Letelier, R.M., Abbott, M.R., 2005. Parameterizing the natural fluorescence kinetics of *thalassiosira weissflogii*. *Limnology and Oceanography* 50 (5), 1499–1510.
- Lehman, J.T., Botkin, D.B., Likens, G.E., 1975. The assumptions and rationales of a computer model of phytoplankton population dynamics. *Limnology and Oceanography* 20 (3), 343–364.
- Ley, A.C., Mauzerall, D., 1982. Absolute absorption cross sections for photosystem II and the minimum quantum requirement for photosynthesis in *Chlorella vulgaris*. *Biochimica et Biophysica Acta* 680, 95–106.
- Lima, I.D., Olson, D.B., Doney, S.C., 2002. Intrinsic dynamics and stability properties of size-structured pelagic ecosystem models. *Journal of Plankton Research* 24 (6), 533–556.
- Moore, C.K., Lucas, M.I., Sanders, R., Davidson, R., 2005. Basin-scale variability of phytoplankton bio-optical characteristics in relation to bloom state and community structure in the Northeast Atlantic. *Deep-Sea Research I* 52, 401–419.
- Moore, C.K. et al., 2003. Physical controls on phytoplankton physiology and production at a shelf sea front: a fast repetition-rate fluorometer based field study. *Marine Ecology Progress Series* 259, 29–45.
- Moore, J.K., Doney, S.C., Lindsay, K., 2004. Upper ocean ecosystem dynamics and iron cycling in a global three-dimensional model. *Global Biogeochemical Cycles* 18, GB4028.
- Newham, L.T.H., Norton, J.P., Prosser, I.P., Croke, B.F.W., Jakeman, A.J., 2003. Sensitivity analysis for assessing the behaviour of a landscape-based sediment source and transport model. *Environmental Modelling & Software* 18, 741–751.
- Oliver, R.L., Whittington, J., Lorenz, Z., Webster, I.T., 2003. The influence of vertical mixing on the photoinhibition of variable chlorophyll *a* fluorescence and its inclusion in a model of phytoplankton photosynthesis. *Journal of Plankton Research* 25 (9), 1107–1129.
- Olson, R.J., Chekalyuk, A.M., Sosik, H.M., 1996. Phytoplankton photosynthetic characteristics from fluorescence induction assays of individual cells. *Limnology and Oceanography* 41 (6), 1253–1263.
- Pawlowski, L., 2004. Modélisation de l'incorporation du Carbone photosynthétique en environnement marin piloté par ordinateur. Ph.D. Thesis, Thèse de Doctorat de l'Université Paris 6.

- Petzold, L.R., 1983. Automatic selection of methods for solving stiff and nonstiff systems of ordinary differential equations. *SIAM Journal on Scientific and Statistical Computing* 4 (1), 136–148.
- Popova, E.E., Fasham, M.J.R., Osipov, A.V., Ryabchenko, V.A., 1997. Chaotic behaviour of an ocean ecosystem model under seasonal external forcing. *Journal of Plankton Research* 19 (10), 1495–1515.
- préising, M., Herodek, S., Preston, T., Vörös, L., 2000. Nitrogen uptake and the importance of internal loading in Lake Balakon. *Freshwater Biology* 46, 125–139.
- Robertson, G.A., Cameron, I., 1997. Analysis of dynamic process models for structural insights and model reduction – part 1: Structural identification measures. *Computers and Chemical Engineering* 21 (5), 455–473.
- Seferlis, P., Hrymak, A.N., 1996. Sensitivity analysis for chemical process optimization. *Computers and Chemical Engineering* 20 (10), 1177–1200.
- Suggett, D., Kraay, G., Holligan, P., Davey, M., Aiken, J., Geider, R., 2001. Assessment of photosynthesis in a spring cyanobacterial bloom by use of a fast repetition rate fluorometer. *Limnology and Oceanography* 46 (4), 802–810.
- Suggett, D., MacIntyre, H.L., Geider, R., 2004. Evaluation of biophysical and optical determinations of light absorption by photosystem II in phytoplankton. *Limnology and Oceanography: Methods* 2, 316–332.
- Thornley, J.H.M., Cannell, M.G.R., 2000. Modelling the components of plant respiration: representation and realism. *Annals of Botany* 85, 55–67.
- Tyystjarvi, E., Aro, E.-M., 1996. The rate constant of photoinhibition, measured in lincomycin-treated leaves, is directly proportional to light intensity. *Proceedings of the National Academy of Sciences of the United States of America* 93, 2213–2218.
- Van den Meersche, K., Middelburg, J.J., Soetaert, K., van Rijswijk, P., Boschker, H.T.S., Heip, C.H., 2004. Carbon–nitrogen coupling and algal–bacterial interactions during an experimental bloom: modeling a ¹³C tracer experiment. *Limnology and Oceanography* 49 (3), 862–878.